

Used Fuel and Uranium Dioxide Dissolution Studies – A Review

NWMO TR-2007-03

July 2007

D.W. Shoemith

The University of Western Ontario

nwmo

NUCLEAR WASTE
MANAGEMENT
ORGANIZATION

SOCIÉTÉ DE GESTION
DES DÉCHETS
NUCLÉAIRES



Nuclear Waste Management Organization
22 St. Clair Avenue East, 6th Floor
Toronto, Ontario
M4T 2S3
Canada

Tel: 416-934-9814
Web: www.nwmo.ca

Used Fuel and Uranium Dioxide Dissolution Studies – A Review

NWMO TR-2007-03

July 2007

D.W. Shoesmith
The University of Western Ontario

Disclaimer:

This report does not necessarily reflect the views or position of the Nuclear Waste Management Organization, its directors, officers, employees and agents (the "NWMO") and unless otherwise specifically stated, is made available to the public by the NWMO for information only. The contents of this report reflect the views of the author(s) who are solely responsible for the text and its conclusions as well as the accuracy of any data used in its creation. The NWMO does not make any warranty, express or implied, or assume any legal liability or responsibility for the accuracy, completeness, or usefulness of any information disclosed, or represent that the use of any information would not infringe privately owned rights. Any reference to a specific commercial product, process or service by trade name, trademark, manufacturer, or otherwise, does not constitute or imply its endorsement, recommendation, or preference by NWMO.

ABSTRACT

Title: Used Fuel and Uranium Dioxide Dissolution Studies – A Review
Report No.: NWMO TR-2007-03
Author(s): D.W. Shoesmith
Company: The University of Western Ontario
Date: July 2007

Abstract

The extensive studies of used fuel dissolution inside a failed nuclear waste container have been reviewed. The primary factor controlling fuel dissolution is the redox condition established at the fuel surface by the radiolysis of water, how it evolves with time as radiation fields decay, and how it is influenced by the presence of oxidant scavengers, especially H_2 , produced by corrosion of the steel liner in the container.

If the container fails early, and oxidizing conditions are established, the fuel dissolution process will be a corrosion reaction driven by radiolytically-produced H_2O_2 . As radiation fields decay and conditions become less oxidizing, the fuel corrosion rate will decrease. The rate, and its evolution with time, will be influenced by the formation of corrosion product deposits, facilitated by calcium and silicate in the groundwater, which lead to the formation of insoluble U^{VI} phases. These deposits could partially block the fuel corrosion process, but could also lead to the formation of locally acidified sites at which the corrosion rate is increased. The location of these sites would be pores in the deposit and/or flaws in the fuel surface. If the groundwater contains sufficient bicarbonate, the formation of deposits would be inhibited and the fuel corrosion process possibly accelerated by the formation of bicarbonate-uranyl ion complexes.

As redox conditions become less oxidizing these issues become less important. The generation of acidity within deposits is unlikely, and since the corrosion rate becomes limited by the available concentration of oxidants, the influence of bicarbonate on the corrosion rate disappears. For sufficiently low radiation dose rates, a threshold for the transition from corrosion to chemical dissolution has been identified electrochemically and validated by dissolution rate measurements on used fuels and alpha-doped UO_2 specimens. For CANDU fuel this threshold is expected to occur between 10,000 and 20,000 years. Beyond this threshold fuel dissolution will be solubility-controlled and extremely slow.

The transition from radiolytic corrosion to chemical dissolution can be very rapidly induced in the presence of oxidant scavengers, especially H_2 . Small concentrations of H_2 suppress the redox condition to the threshold even for used fuels with high gamma/beta radiation fields. For sufficiently high concentrations, the establishment of the reversible H_2/H^+ reaction on noble metal epsilon particles can lead to galvanic protection of the fuel against corrosion. It is possible that this effect could lead to protection of the fuel against corrosion almost from the time of container failure. Under these conditions fuel dissolution and radionuclide release would be extremely small.

TABLE OF CONTENTS

	<u>Page</u>
ABSTRACT	v
1. INTRODUCTION	1
2. DESCRIPTION OF USED FUEL	2
3. PROCESSES CONTROLLING FUEL MATRIX DISSOLUTION	5
4. FUEL CORROSION THRESHOLD	8
5. KEY INFLUENCES DETERMINING THE FUEL CORROSION RATE.....	12
6. COMPOSITION OF THE FUEL SURFACE	13
7. REACTIVITY OF THE FUEL SURFACE.....	14
8. INFLUENCE OF CORROSION PRODUCT DEPOSITS	16
8.1 Influence of Redox Conditions and Groundwater Speciation on the Nature of Surface Deposits	17
8.2 Development of Local Acidity at the Corroding Fuel Surface	22
8.3 The Influence of Carbonate on Fuel Corrosion	26
9. KINETICS OF REDUCTION OF CATHODIC REAGENTS	28
9.1 Kinetics of Oxygen Reduction	28
9.2 Kinetics of Hydrogen Peroxide Reduction.....	31
10. THE INFLUENCE OF REDOX SCAVENGERS PRODUCED BY CARBON STEEL CORROSION	33
10.1 Scavenging by Ferrous (Fe^{II}) Ions	34
10.2 Scavenging by Hydrogen	35
11. FUEL CORROSION/DISSOLUTION RATES	40
12. CONCLUSIONS	44
ACKNOWLEDGEMENTS.....	46
REFERENCES	46

LIST OF FIGURES

	<u>Page</u>
Figure 1: Illustration showing a deep geologic repository concept for used nuclear fuel	1
Figure 2: Typical CANDU fuel bundle	2
Figure 3: A - Scanning electron microscope photographs of UO ₂ fuel. B - Optical micrographs of polished and etched UO ₂ fuel, and of the segregation of metallic fission products from the UO ₂	3
Figure 4: Cut away view of a used fuel container showing the inner and outer vessels and the fuel bundles.....	4
Figure 5: Illustration demonstrating the thermodynamic driving force for fuel corrosion in an aqueous solution containing oxidants.....	6
Figure 6: Illustration showing the radiolytic production of oxidants by the alpha, beta, gamma radiolysis of water, and the coupling of cathodic oxidant processes to anodic fuel dissolution, which constitutes the overall fuel corrosion process	7
Figure 7: Alpha, beta, and gamma radiation dose rates calculated as a function of time for a layer of water in contact with a CANDU fuel bundle with a burnup of 220 MWh/kg U	8
Figure 8: The fractions of various oxidation states of uranium in a 1.5 wt% SIMFUEL electrode surface as a function of electrochemical potential.....	10
Figure 9: The composition of a UO ₂ surface as a function of potential (from Figure 8)	10
Figure 10: Illustration showing the concept of an alpha activity threshold for the onset of radiolytically-controlled fuel corrosion	11
Figure 11: Illustration showing the key reactions anticipated inside a groundwater flooded waste container	12
Figure 12: Raman spectra recorded on three SIMFUEL specimens with different degrees of simulated burnup	15
Figure 13: Anodic currents recorded on three SIMFUEL electrodes with different degrees of simulated burnup in 0.1 mol/L NaCl (pH=9.5).....	15
Figure 14: Illustration showing a porous deposit on a corroding surface exposed to an aqueous environment.....	17

Figure 15: Illustrations showing the influence of a corrosion product deposit on the local chemistry at the corroding fuel surface	18
Figure 16: Anodic dissolution charges measured on a 1.5wt% SIMFUEL in a 0.1 mol/L solution (pH = 9.5) containing different ratios of CaCl ₂ and NaCl.....	19
Figure 17: The relative fractions of the three uranium oxidation states in the surface of a 1.5wt% SIMFUEL electrode as a function of the fraction of Ca ²⁺ present in a NaCl/CaCl ₂ solution with an overall concentration of 0.1 mol/L (pH = 9.5).....	20
Figure 18: A - Atomic percentage of Si on the surface of an electrochemically-oxidized 1.5wt% SIMFUEL electrode. B - Correlation between the amounts of U ^{VI} and silicate on the SIMFUEL surface	20
Figure 19: Scanning electron microscopy (SEM) image and energy dispersive X-ray (EDS) maps of a 1.5 wt% SIMFUEL surface slowly electrochemically oxidized in a solution containing 0.1 mol/L NaSiO ₃ + 0.1 mol/L NaCl (pH = 9.5)	21
Figure 20: Possible secondary phases that could form under different redox conditions on a corroding/ dissolving UO ₂ surface.....	22
Figure 21: Illustrations showing how acidity can develop within pores in a corrosion product deposit	23
Figure 22: A - Illustration showing the electrochemical, chemical, and transport processes considered in a model to predict the pH at the bottom of a pore in a corrosion product (UO ₃ xH ₂ O) deposit on a corroding UO ₂ surface. B - Illustration showing the axial symmetry assumed for the pore, and the hydrolysis reactions involved in generating acidity	24
Figure 23: The pH predicted at the base of a pore in a corrosion product deposit as a function of pore depth, and the potential at which dissolution was occurring	25
Figure 24: The influence of the maximum pH change predicted at the base of a 300µm deep pore on UO ₂ dissolution occurring at a potential of 300mV.....	25
Figure 25: Measured dissolution rates of UO ₂ as a function of pH in a 0.1mol/L NaClO ₄ solution purged with gas containing various percentages of O ₂	26
Figure 26: Steady-state electrochemical dissolution currents measured on a 1.5 wt % SIMFUEL electrode as a function of applied potential in a 0.1mol/L NaCl solution (pH=9.7) containing various concentrations of HCO ₃ ⁻ /CO ₃ ²⁻	27
Figure 27: Schematic illustrations indicating the influence of various factors on O ₂ reduction on UO ₂ surfaces (Shoesmith 2000).....	29
Figure 28: O ₂ reduction currents recorded on various SIMFUEL electrodes in a 0.1mol/L NaCl (pH=9.5) solution purged with air ([O ₂]=2.5 x 10 ⁻⁴ mol/L.....	30

Figure 29: Illustration showing the H ₂ O ₂ decomposition reaction catalyzed on a non-stoichiometric UO _{2+x} surface	31
Figure 30: Illustration showing how H ₂ O ₂ decomposition is blocked on an oxidized UO ₂ surface.....	32
Figure 31: Illustrations showing that H ₂ O ₂ reduction is rapid on both the fuel surface and epsilon particles, while the reduction of O ₂ is only rapid on epsilon particles	33
Figure 32: Illustration showing the two corrosion fronts existing within a failed, groundwater flooded waste container, one on the fuel surface established by reaction with radiolytic oxidants and a second one on the steel surface established by reaction with water.....	34
Figure 33: Time dependence of the corrosion potential (E _{CORR}) of a UO ₂ electrode in gamma-irradiated 0.1 mol/L NaCl (pH~9.5) at room temperature in the presence of either 5MPa of H ₂ or Ar	37
Figure 34: Corrosion potential (E _{CORR}) values measured on UO ₂ at 5 MPa of H ₂ , and on 1.5 at % SIMFUEL at various H ₂ pressures, compared to the ranges of values measured under various anoxic and oxidizing conditions	38
Figure 35: The influence of H ₂ solution overpressure on the corrosion potential of a 1.5 at% SIMFUEL containing epsilon particles (A) and a 1.5 at% SIMFUEL with no epsilon particles (B)	39
Figure 36: The influence of the increasing number and size of epsilon particles in SIMFUELS with different degrees of simulated burnup on the corrosion potential (E _{CORR}) and the degree of oxidation of the surface in H ₂ -purged 0.1 mol/L KCl	39
Figure 37: Illustration showing the galvanic coupling of epsilon particles to the fuel matrix in H ₂ -containing solutions	40
Figure 38: Corrosion rates measured as a function of specific alpha activity on alpha-doped electrodes, undoped UO ₂ (10 ⁻² M Bq/g) and spent fuel (Figure 25 in Poinssot et al. 2005).....	41
Figure 39: Alpha, beta and gamma radiation dose rates calculated as a function of time for a layer of water in contact with a CANDU fuel bundle with a burnup of 220 MWh/kg U	42
Figure 40: Used fuel dissolution rates, based on dissolved ²³⁸ U and ¹³⁷ Cs concentrations as a function of pH for oxidizing and reducing conditions	43

1. INTRODUCTION

The recommended approach for long-term management of used nuclear fuel in Canada is the Adaptive Phased Management approach (NWMO 2005). This approach includes centralized containment and isolation of the used fuel in a deep geological repository in a suitable rock formation. The Canadian repository concept is based on multiple barriers: the used fuel bundles, durable metal containers, a clay buffer and seals around each container, and a deep stable geologic environment. An illustration of a recent repository concept is shown in Figure 1 (McMurry et al. 2003).

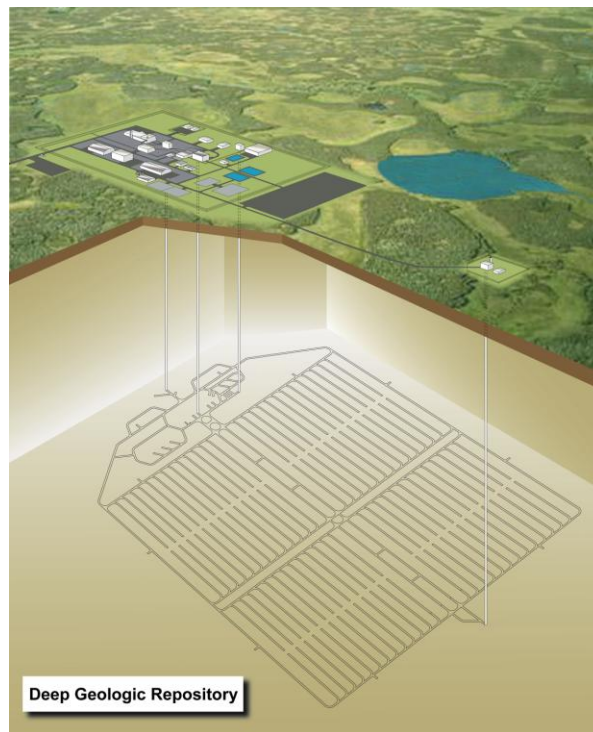


Figure 1: Illustration showing a deep geologic repository concept for used nuclear fuel.

This deep geologic repository can provide reasonable assurance in the long-term containment and isolation of the used fuel bundles, an assurance considerably enhanced by the selection of a copper-shell container (McMurry et al. 2000; King and Kolar 2000; King and Kolar 1996; Maak 2003). However, it is judicious to assume containers will eventually fail, thereby exposing the used fuel bundles to groundwater. Furthermore, although the thin Zircaloy cladding on the fuel is likely to provide a further barrier, it is usually conservatively assumed that groundwater can contact the used fuel directly.

Since the used fuel contains the residual radioactivity, its behaviour on contact with groundwater is important for long-term safety assurance. Over the past 25-30 years, a substantial effort has been expended internationally to study fuel dissolution and radionuclide release processes under a range of proposed waste repository conditions (Johnson and

Shoesmith 1988; Shoesmith 2000; Johnson et al. 1994; Johnson et al. 1996; Shoesmith et al. 2005). This report will review the present understanding of the fuel corrosion/dissolution process.

2. DESCRIPTION OF USED FUEL

CANDU fuel pellets are fabricated from high-purity unenriched UO_2 ($^{235}\text{U} = 0.71\%$) with a typical grain size of $5 - 10 \mu\text{m}$, approach 97% of theoretical density, and are close to stoichiometry ($\text{UO}_{2.001}$) in composition. The pellets are sealed within a Zircaloy-4 (Zr-Sn) sheathing (cladding), and assembled into bundles. A typical bundle design is shown in Figure 2. On removal from reactor, the radioactivity, thermal heat output, and composition of the fuel are roughly proportional to its burnup; the energy released per unit mass of uranium. The typical burnup range for CANDU fuel is ~ 120 to 320 MWh/kgU and a reference value of 220 MWh/kgU has been used in recent repository studies (Tait et al. 2000).

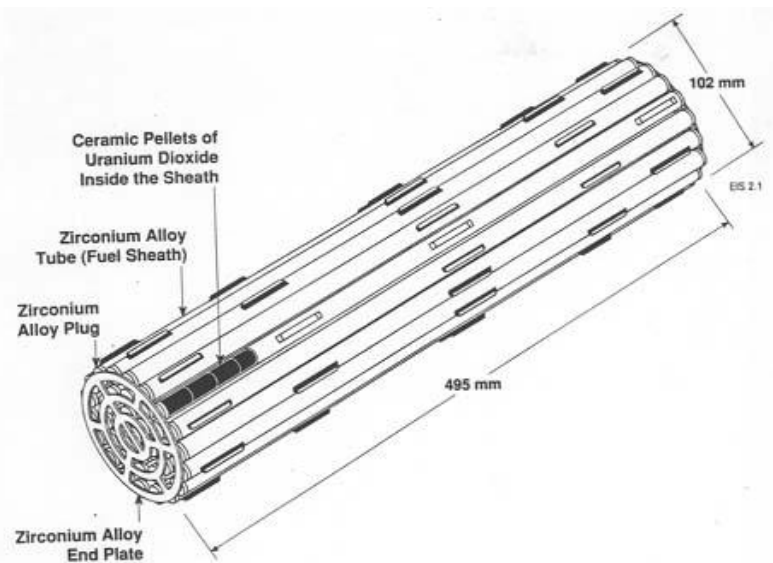


Figure 2: Typical CANDU fuel bundle

The fuel undergoes a number of microstructural and compositional changes during in-reactor use, as illustrated in the sequence of photographs in Figure 3A (McMurry et al. 2000). Un-irradiated UO_2 fuel possesses a cohesive, interlocking microstructure with some internal sintering porosity remaining from the fuel fabrication process. During in-reactor irradiation, the sintering porosity left behind in the UO_2 grains by the fuel fabrication process is largely eliminated. The individual grains grow, a process accompanied by the redistribution of non-volatile fission products within the UO_2 fuel matrix, some of which form small metallic particles (epsilon (ϵ) particles) at grain boundaries. Volatile fission products can diffuse out of grains to form gas bubbles at grain boundaries. These features are illustrated in the optical micrographs in Figure 3B.

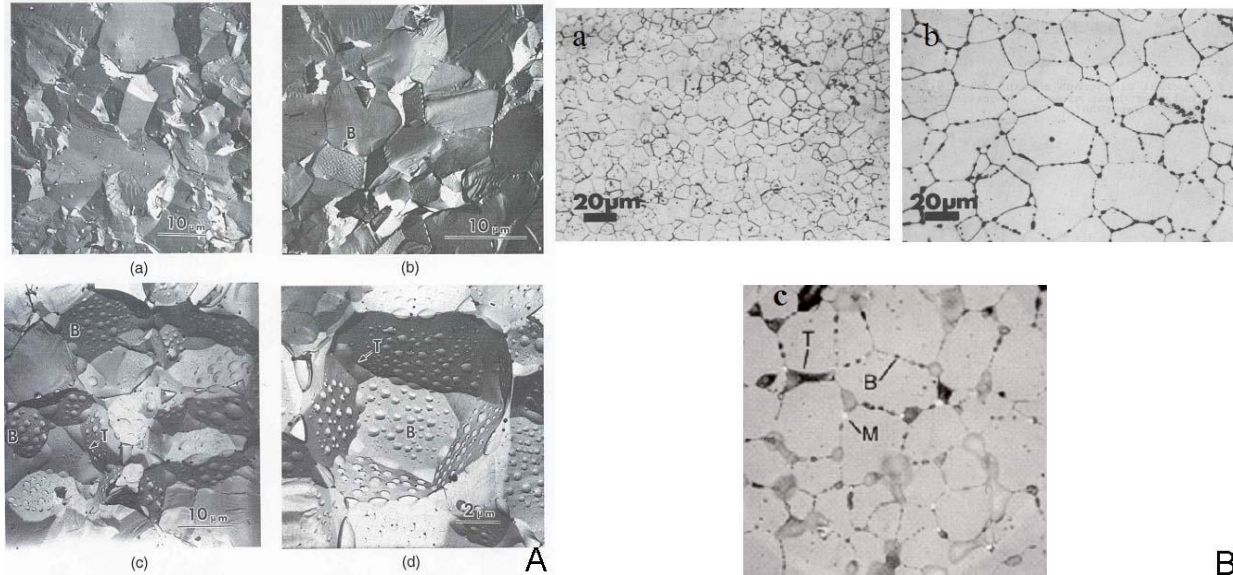


Figure 3: A - Scanning electron microscope photographs of UO_2 fuel (Hastings 1982)

- (a) Typical microstructure of unirradiated UO_2 . Small inclusions = sintering porosity.
- (b) Irradiated at low power ($< 45 \text{ kW/m}$). Note the loss of sintering porosity and the development of small intergranular fission gas bubbles (B).
- (c) Irradiated at higher power ($\geq 50 \text{ kW/m}$), showing growth of fission gas bubbles (B) and the initiation of tunnels (T).
- (d) Magnified view of irradiated higher power fuel. Note the grain-edge tunnels (T) and the development of fission gas bubbles (B) on all faces of the empty grain location.

Figure 3: B - Optical micrographs of polished and etched UO_2 fuel (Hastings 1982) **and of the segregation of metallic fission products from the UO_2** (Novak and Hastings 1991)

- (a) Unirradiated UO_2 . Note sintering porosity in grain interiors.
- (b) Irradiated UO_2 at low burnup (20 MWh/kgU at 50 kW/m). Note the increase in grain size (equiaxial grain growth), the loss of sintering porosity, and the development of fission gas bubbles and tunnels along boundaries.
- (c) Irradiated UO_2 at high burnup (770 MWh/kgU at 52 kW/m), showing small white particles at grain boundaries that are formed from incompatible metals such as Mo, Ru, and Pd that have diffused out of the UO_2 grains. Well-developed fission gas bubbles (B) and tunnels (T) are also present at grain boundaries. The scale is approximately the same as in (b).

The radionuclides within used fuel are primarily from fission products and actinides, but small quantities of activated lighter elements will also be present. The radionuclides within the used fuel can be grouped into three distinct categories:

- 1) Fission products which are volatile at reactor operating temperatures, and migrate during reactor operation to the fuel/sheath gap.
- 2) Fission products, which migrate to grain boundaries, and reside there in fission gas bubbles, or separate into solid phases such as perovskites ((Ba, Sr) ZrO₃) and metallic epsilon (ε) particles (Mo, Ru, Rh, Pd, Tc).
- 3) Fission products and actinides/lanthanides that are retained in the fuel matrix.

On exposure to groundwater within a failed container, the fission products in categories 1 and 2 are assumed to dissolve quickly into the ground water as illustrated in Figure 4. For fission products in category 1, this assumption is realistic since they are inevitably soluble and completely unretained by the fuel matrix. For fission products in category 2, such an assumption is conservative, since the grain boundaries are not immediately accessible to groundwater, and release of radionuclides from these locations could be controlled to a significant degree by the corrosion/dissolution of the fuel. Radionuclides in categories 1 and 2 are termed the instant release fraction. Discussions of the instant release fraction, and how it is determined, are available elsewhere (McMurry et al. 2000; Johnson et al. 1994; Garisto et al. 2004; Werme et al. 2004).

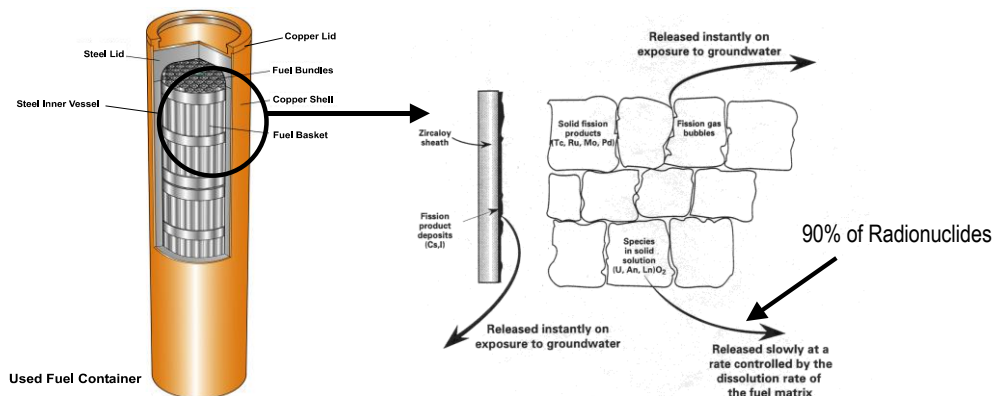


Figure 4: Cut away view of a used fuel container showing the inner and outer vessels and the fuel bundles (McMurry et al. 2003). Also shown is a schematic illustration of the three distinct categories of fission products and actinides; the gap and grain boundary inventories that constitute the Instant Release Fraction (IRF), and the matrix inventory, whose release will be controlled by fuel corrosion/ dissolution.

The great majority of radionuclides (> 90%) are retained within the fuel matrix; i.e., category 3. Since these are embedded within the dense UO₂ grains, they can only be released by diffusion to the grain boundaries or by dissolution of the UO₂ grains themselves. Solid-state diffusion is slow at repository temperatures (< 100°C), making used fuel corrosion or dissolution the primary process for the release of this majority of radionuclides.

3. PROCESSES CONTROLLING FUEL MATRIX DISSOLUTION

The release of the > 90% of radionuclides contained within the solid-state matrix of the used fuel will be governed by the corrosion/dissolution of the UO_2 matrix. The rate of this process will be related to, but not necessarily directly proportional to, the solubility of uranium in the groundwater. At repository depths, groundwaters are inevitably oxygen-free and any oxygen introduced during repository construction and operation prior to sealing will be rapidly consumed by mineral and biochemical reactions in the surrounding clays and by minor corrosion of the copper container (McMurry et al. 2000; King et al. 2000; King et al. 1996; Maak et al. 2003). The groundwater chemistry will depend on its origin in the host rock. For relevant Canadian Shield crystalline rock, it is expected to be $\text{Ca}^{2+}/\text{Na}^+/\text{Cl}^-/\text{SO}_4^{2-}$ dominated with a pH in the range 6 to 9 (McMurry et al. 2003). It may also contain small amounts of HCO_3^- (10^{-4} to 10^{-3} mol/L).

For these neutral anoxic conditions, the theoretical solubility of crystalline UO_2 , calculated from thermodynamic data, is extremely low ($\sim 10^{-15}$ mol/L) (Werme et al. 2004). However, measurements (Parks and Pohl 1988; Grenthe et al. 1992; Fuger 1993; Neck and Kim 2001; Rai et al. 2003; Yajima et al. 1995; Rai et al. 1990; Guillamont et al. 2003) yield values of the order of $\sim 10^{-9.5}$ mol/L for $\text{pH} > 4$ (due to formation of amorphous UO_2 during the experiments). Above $\text{pH} = 4$, the solubility is insensitive to pH. Since there is some variation in measured solubilities depending on the degree of crystallinity of the solid, the OECD-NEA recommended value is $10^{-8.5}$ mol/L (Guillamont et al. 2003).

These solubilities are for uranium in the +4 oxidation state (U^{IV}), its normal condition in stoichiometric UO_2 . The corresponding solubility equilibrium is



If the concentration of dissolved U^{IV} is controlled at the fuel surface by this solubility equilibrium, then the fuel dissolution rate will be controlled by the diffusive or advective transport of U away from the fuel. Early Canadian safety assessment models, e.g., the first AECL case study (Johnson et al. 1994), focused on such a solubility limited transport controlled model (Lemire et al. 1989; Garisto et al. 1991; King et al. 2000). Solubilities calculated with this model were consistent with the range of measured solubilities and the rate of release of those radionuclides contained within the fuel matrix (category 3) was predicted to be very slow.

While groundwater entering the failed container may be anoxic, its radiolysis due to the residual radioactivity from the fuel will produce a variety of chemical species including oxidants. These species are produced directly at, or in the environment immediately adjacent to, the fuel surface once it is wetted with groundwater. The possibility that water radiolysis could produce oxidizing conditions has stimulated a revised approach to the modeling of used fuel dissolution. This is the background behind current Canadian used fuel models, like those used in AECL's second case study (Johnson et al. 1996) and Ontario Power Generation's third case study (Garisto et al. 2004; Gierszewski et al. 2004).

Under oxidizing conditions, UO_2 can be oxidized to the +6 oxidation state (U^{VI}), e.g., as UO_2^{2+} , and dissolve since the solubility of U in the U^{VI} state is many orders of magnitude greater than in the U^{IV} state (as UO_2) (Grenthe et al. 1992). It is now universally acknowledged that in the presence of oxidants, this dissolution process must be considered a corrosion reaction, in which

the oxidant is consumed to convert the insoluble U^{IV} (in UO_2) to the much more soluble U^{VI} (as UO_2^{2+}).

The rate of this reaction will depend on redox conditions (Shoesmith 2000; Johnson et al. 1996; Werme et al. 2004; Shoesmith et al. 2003; Sunder et al. 1997; Shoesmith et al. 1998; King et al. 1999; Sunder 1995; Carbol et al. 2005). The thermodynamic driving force for a corrosion process is illustrated in Figure 5. The redox potential of the groundwater ($E_{Red/Ox}$, commonly termed E_h) must be more positive than the equilibrium potential for fuel dissolution ($(E^e)_{UO_2/UO_2^{2+}}$). The driving force for corrosion is the potential difference, $E_{Red/Ox} - (E^e)_{UO_2/UO_2^{2+}}$. Under such conditions the fuel will establish a corrosion potential (E_{CORR}) at which the anodic fuel dissolution rate ($UO_2 \rightarrow UO_2^{2+} + 2e^-$), termed the corrosion rate, will be equal to the rate of the oxidant reduction reaction ($Ox + 2e^- \rightarrow Red$), as illustrated schematically in Figure 6.

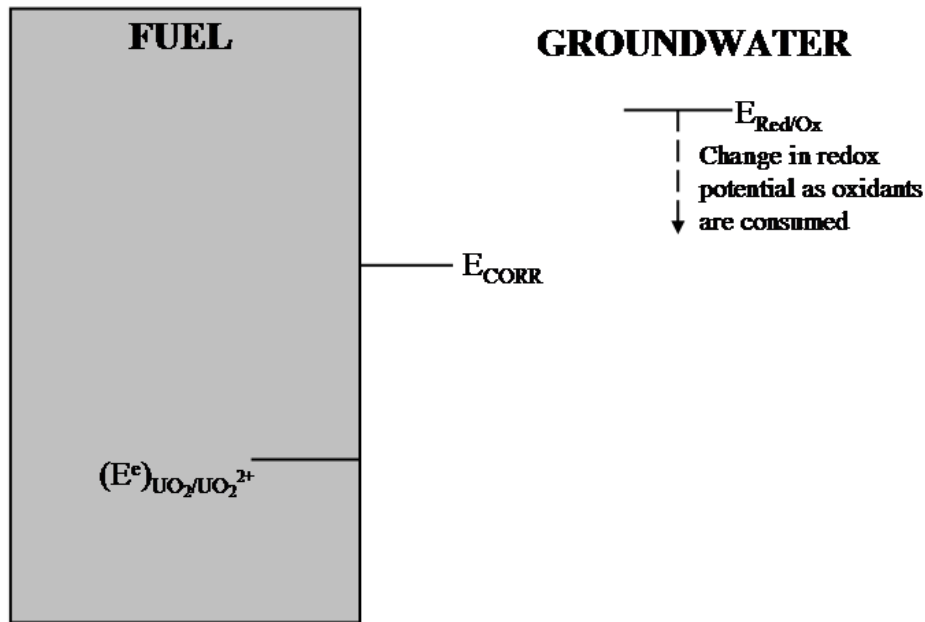


Figure 5: Illustration demonstrating the thermodynamic driving force for fuel corrosion in an aqueous solution containing oxidants. E_{CORR} is the corrosion potential at which the overall process takes place on the fuel surface.

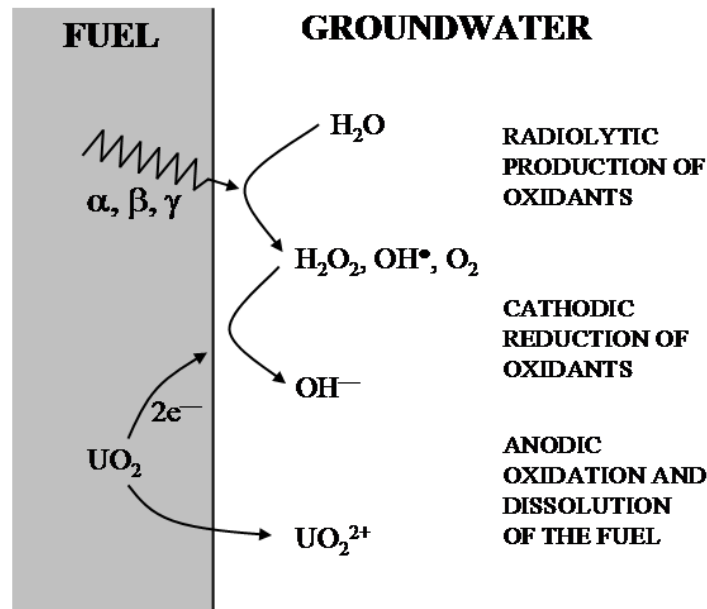


Figure 6: Illustration showing the radiolytic production of oxidants by the alpha, beta, gamma radiolysis of water, and the coupling of cathodic oxidant processes to anodic fuel dissolution which constitutes the overall fuel corrosion process.

The sum of these two “half” reactions constitutes the overall corrosion process,



and the corrosion rate will be controlled by the kinetics of the slowest “half” reaction.

As shown in Figure 7, the radiation fields associated with the used fuel will decay with time, leading to a decrease in the radiolytic oxidant concentrations, and, therefore, a decrease in $E_{Red/Ox}$ (E_h). This will lead to a decrease in both E_{CORR} and the fuel corrosion rate as the driving force for corrosion is reduced by the consumption of oxidants and the decreasing rate of their replenishment. If $E_{Red/Ox}$ were to fall to a value less than $(E^e)_{UO_2/UO_2^{2+}}$, then corrosion would become thermodynamically impossible and only chemical dissolution (via reaction 1) could occur.

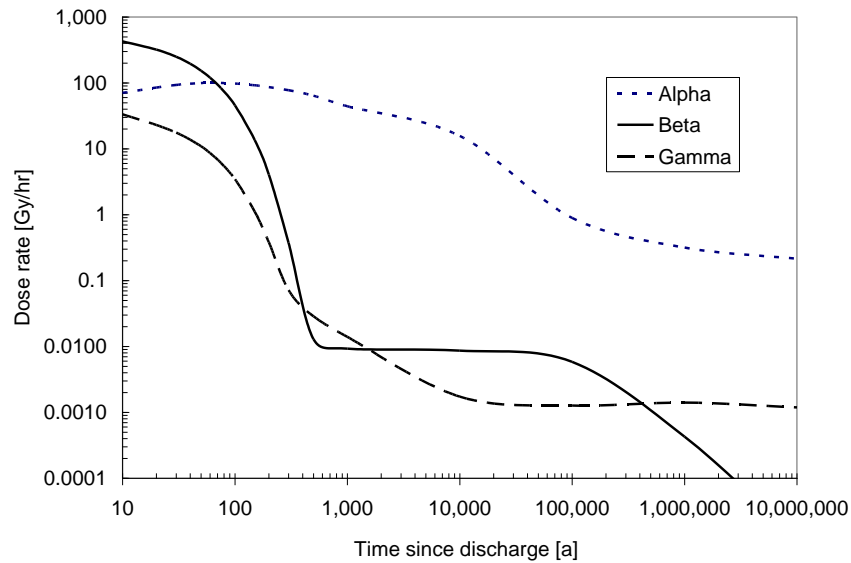


Figure 7: Alpha, beta, and gamma radiation dose rates calculated as a function of time for a layer of water in contact with a CANDU fuel bundle with a burnup of 220 MWh/kgU.

This evolution in solution redox conditions (E_h) makes the fuel corrosion process (and, hence, the radionuclide release process) very dependent on the time to failure of the waste container. Clearly, the longer the period of containment to prevent wetting of the fuel, the lower the rate of production of radiolytic oxidants and, hence, the lower the thermodynamic driving force for fuel corrosion. If the corrosion rate, and its evolution with time, is then to be determined it is necessary to know the time groundwater contacts the fuel, the redox conditions in the groundwater established by water radiolysis, whether these conditions are sufficiently oxidizing to support fuel corrosion, and a measured relationship between redox condition and fuel corrosion rate.

4. FUEL CORROSION THRESHOLD

The dependence of fuel corrosion rate (and E_{CORR}) on redox conditions is now well established, based on electrochemical measurements (Shoesmith 2000; Johnson et al. 1996, Shoesmith et al. 1991; Sunder et al. 2004; Shoesmith et al. 1998), measurements of corrosion rates (or rate constants) in the presence of oxidants (Ekeroth et al. 2003; Hossain et al. 2006; Gimenez et al. 1996; de Pablo et al. 1996; de Pablo et al. 2001; Clarens et al. 2004; Corbel et al. 2006; de Pablo et al. 2004), and measurements in the presence of radiation fields (Carbol et al. 2005; Corbel et al. 2006; Jegou et al. 2004; Mennecart et al. 2004; Stroes-Gascoyne et al. 2005; Bailey et al. 1985; Sunder et al. 1992; Sunder et al. 1997; Wren et al. 2005).

Thermodynamically, it is also straightforward to determine the surface redox conditions when UO_2 should be immune to corrosion and, hence, susceptible only to chemical dissolution. Using the available data (Grenthe et al. 1992; Paquette et al. 1981; Lemire et al. 1980), E_h (and hence, E_{CORR}) would have to be less than -0.35V (vs. the saturated calomel electrode (SCE)) at a groundwater pH of 9.5 (and would decrease by 0.06V for each unit increase in pH). However,

given the complexity of the solid-state chemistry of UO_2 and its evolution during in-reactor irradiation, it is judicious to establish an oxidative (corrosion) threshold experimentally. Knowledge of this threshold is essential if the influence on fuel corrosion of redox active species in the groundwater is to be accurately assessed. This is particularly important considering the experimentally demonstrated influence of redox scavengers, Fe^{2+} and H_2 , produced within a failed, groundwater flooded, waste container.

Uranium can exist in three different oxidation states, U^{IV} , U^{V} , and U^{VI} , but is effectively only soluble as U^{VI} , and then only to a concentration of approximately 10^{-5} mol/L in neutral pH solutions (Grenthe et al. 1992; Guillaumont et al. 2003). Using electrochemical methods, and subsequently analyzing the surface by X-ray photoelectron spectroscopy (XPS), the composition of the fuel surface has been carefully mapped as a function of fuel surface potential. Figure 8 clearly shows the increasing oxidation of the surface for potentials above approximately -0.3V . At potentials below this value, the relative amounts of the three oxidation states present are identical to those observed for reduction of the surface at very negative potentials (-1.5V). The small amounts of oxidized states, U^{V} and U^{VI} , observed at applied potentials $< -0.4\text{V}$ can be attributed to an unavoidable slight air oxidation of the surface on transfer from the electrochemical cell to the vacuum chamber of the spectrometer.

All three oxidation states of U can be detected, and their relative proportions vary with applied potential (Broczkowski et al. 2007; Santos et al. 2004; Shoesmith et al. 2004). The U^{V} state exists only as an intermediate in the overall anodic (oxidative) dissolution process. As indicated in the reaction scheme across the top of this figure, the top few nanometers of the surface are converted to a mixed $\text{U}^{\text{IV}}/\text{U}^{\text{V}}$ oxide (UO_{2+x}) prior to conversion to the more soluble U^{VI} state. Since the oxidation state of the U in the surface has increased, oxygen anions (O^{II}) are injected into the fuel lattice to maintain charge neutrality. As will be discussed below, this thin surface layer has catalytic properties, and is important in determining the kinetics of the overall corrosion process. As the potential increases, the rate of oxidation and dissolution of the fuel surface increases exponentially with applied potential (Shoesmith 2000) and the slightly soluble U^{VI} exceeds its solubility product at the fuel surface and deposits as $\text{UO}_3 \cdot y\text{H}_2\text{O}$. The behaviour at very high potentials will be discussed below.

Based on this data, and additional electrochemical evidence (Santos et al. 2004; Shoesmith et al. 2004), the evolution of the fuel surface composition can be specified as a function of potential, Figure 9. In this plot, the potential axis is labelled E_{CORR} , and represents the response of the fuel surface to the redox condition (E_h) in the exposure environment. Much of the detail in these two figures will be addressed below. Here, it is noted that the onset of oxidation occurs around -0.3 to -0.4V , i.e., within the region expected thermodynamically, and is relatively insensitive to temperature. The vertical dashed line is conservatively drawn at -0.4V to represent the threshold for the onset of fuel corrosion. Above this potential there is the possibility of fuel corrosion at a rate controlled by the concentration of radiolytically produced oxidants. For potentials below this threshold, fuel dissolution, and hence the mobilization of radionuclides, can only occur by chemical dissolution, e.g., via reaction 1.

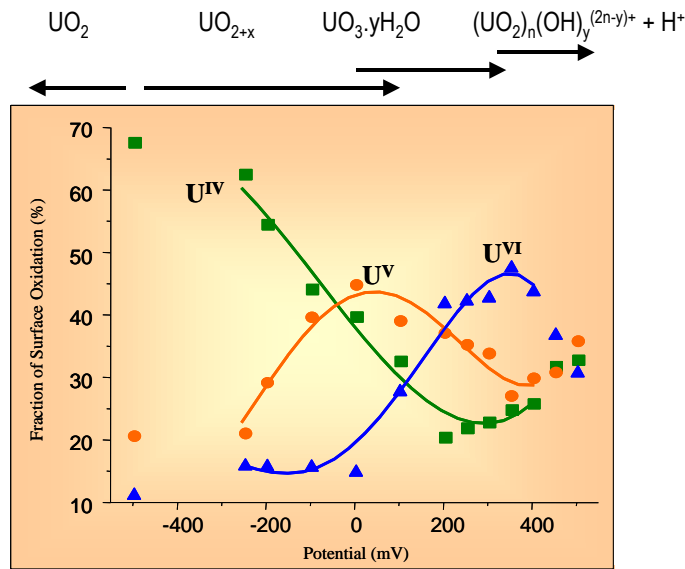


Figure 8: The fractions of various oxidation states of uranium in a 1.5 wt% SIMFUEL electrode surface as a function of electrochemical potential. The electrode was anodically oxidized at each potential for 1 hour in 0.1mol/L (NaCl (pH=9.5) and then analyzed by x-ray photoelectron spectroscopy (XPS) [Santos et al. 2004].

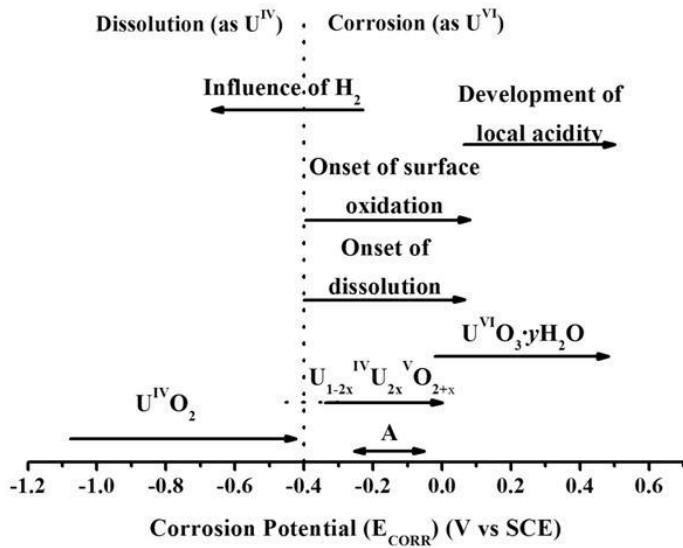


Figure 9: The composition of a UO₂ surface as a function of potential (from Figure 8). The vertical dashed line indicates the potential threshold above which UO₂ would be expected to be subject to corrosion, and below which only chemical dissolution can occur. The arrow A indicates the corrosion potential range predicted by a mixed potential model to describe fuel corrosion due to the alpha radiolysis of water inside a failed waste container (Shoesmith and King 2003)). The upper limit of this range represents the expected E_{CORR} if the container fails on emplacement, and the lower limit represents the E_{CORR} predicted after 10⁶ years.

A similar effort to identify this threshold, based on the measurements of E_h and dissolved U concentrations in experiments employing α -doped material (^{233}U or ^{238}Pu), was undertaken within a recent spent fuel project in Europe (Poinssot et al. 2005). U dissolution rates were found to decrease with decreasing specific alpha activity in the fuel specimen, and there appeared to be a specific activity threshold below which no influence of alpha radiolysis could be detected. It was claimed that above this threshold, fuel dissolution was radiolytically controlled (i.e., a corrosion process) while below it, dissolution was solubility-controlled (i.e., a chemical reaction) as illustrated in Figure 10. Solubility-control was assumed to be established for dissolved U concentrations $< 10^{-9}$ mol/L (comparable to the OECD-NEA recommended value of $10^{-8.5}$ mol/L for the solubility of UO_2), E_h values $< -0.01\text{V}$ (-0.25V on the SCE scale used in Figure 9), and the observation in long term tests that the U concentration did not increase with time.

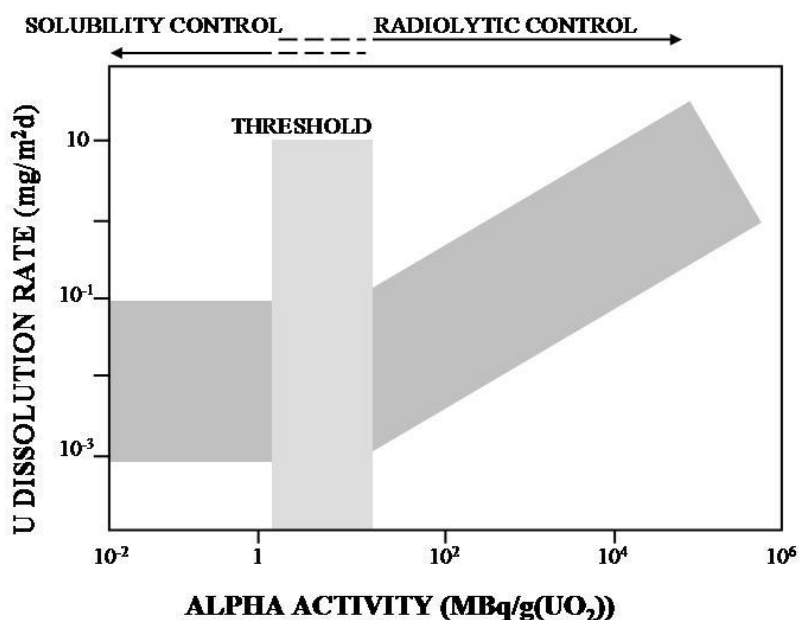


Figure 10: Illustration showing the concept of an alpha activity threshold for the onset of radiolytically-controlled fuel corrosion. Below the threshold, the fuel dissolution process is solubility-controlled. The darker shaded areas illustrate the spread in measured rates of the influence of alpha activity on fuel corrosion (adapted from Figure 25 in Poinssot et al. 2005, see also Figure 38 in this report).

Since corrosion will not occur in the absence of oxidants, E_h and E_{CORR} should both decrease towards the equilibrium potential as radiation fields decay. Thus, E_h at the alpha activity threshold (Figure 10) and E_{CORR} at the electrochemical threshold (Figure 9) should approach the same value. While E_h from the α -doped fuel experiments has not been measured at $\text{pH} = 9.5$ (the value used to obtain the data in Figure 10), the measured pH dependence (over the range $6 \leq \text{pH} \leq 8$ (Poinssot et al. 2005)) of E_h suggests a value at $\text{pH} = 9.5$ in the region of -0.1V (-0.35V vs. SCE) which compares well with the threshold defined in Figure 9. Considering

the distinctly different experimental approaches used, the two threshold values are gratifyingly consistent.

5. KEY INFLUENCES DETERMINING THE FUEL CORROSION RATE

While the above measurements and considerations establish the basic corrosion nature of the fuel dissolution process and its dependence on redox conditions in the presence of radiolytically decomposed water, a much clearer understanding of the chemistry/electrochemistry involved is required to justify long-term predictions for safety assessment calculations. The key reactions anticipated within a failed, groundwater-flooded container have been defined using the mixed potential model (MPM), a model based on electrochemical principles and the extensive electrochemical database available (Shoesmith et al. 2003; Shoesmith et al; 1998), and are summarized in Figure 11. In this model the Zircaloy cladding is conservatively assumed to provide little or no protection of the fuel against contact with groundwater, and reasonably assumed to be inert and chemically uninvolved in the reactions described.

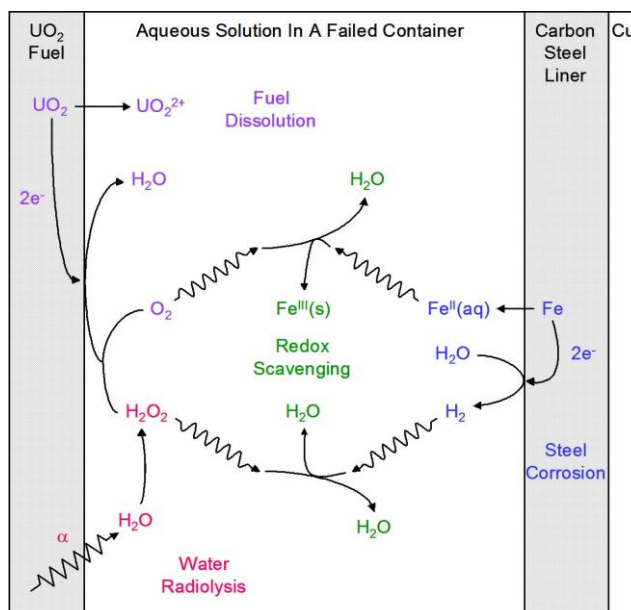


Figure 11: Illustration showing the key reactions anticipated inside a groundwater flooded waste container.

Two corrosion fronts exist, one on the fuel surface and a second one on the surface of the carbon steel liner. On the fuel surface, corrosion is driven by reaction of UO_2 with the products of water radiolysis. If the container and cladding are reasonably assumed to prevent wetting of the fuel surface until γ/β radiation fields have decayed to insignificant levels (within 1000 years, Figure 7), the source of oxidants will be the alpha radiolysis of water. This makes H_2O_2 the primary oxidant available to drive fuel corrosion (Ekeroth et al. 2003; Ekeroth et al. 2006; Nielson et al; 2006), although the production of O_2 via H_2O_2 decomposition would introduce a second oxidant (see below).

On the steel surface, corrosion can be sustained by reaction with water to produce Fe^{2+} and H_2 . Since these corrosion fronts are interconnected by diffusion processes in the groundwater, many possibilities exist for homogenous redox reactions between radiolytic oxidants and soluble fuel and steel corrosion products, leading to the precipitation and redissolution of U and Fe solid phases, and the possibility of adsorption/desorption processes on these solids. A more complete description of possible reactions is given elsewhere (Shoesmith et al. 2003; Shoesmith et al; 1998).

Based on this scheme, and calculations and sensitivity analyses performed using the model (King et al. 1999; King et al. 2000; King et al. 2001a; King et al; 2001b; King et al; 2002; King et al. 2002b; Kolar et al. 2003), the following key issues were identified:

- 1) The composition and reactivity of the fuel surface as a function of redox condition;
- 2) The influence of groundwater species and corrosion product deposits on the fuel surface;
- 3) The kinetics of $\text{H}_2\text{O}_2/\text{O}_2$ reduction in support of fuel corrosion; and
- 4) The scavenging of radiolytic oxidants and/or the inhibition of their reaction with the fuel surface by the products of steel corrosion, particularly H_2 .

6. COMPOSITION OF THE FUEL SURFACE

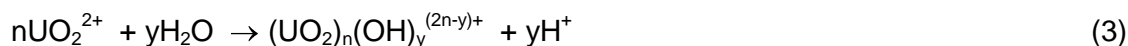
Figure 8 illustrates that the composition of the surface changes as the potential is increased through the corrosion region (i.e., for potentials greater than the threshold of -0.4 V). Since redox conditions inside a failed container will change as radiation fields decay with time, E_{CORR} and, hence, the composition of the surface, would also be expected to change and influence the corrosion process.

Over the potential range from the threshold at -0.4V to approximately 0V (the actual value depends somewhat on temperature (Broczkowski et al. 2007)), the U^{V} content of the UO_{2+x} surface layer increases with potential. Since the conductivity of UO_2 increases as x in UO_{2+x} increases (Hyland et al. 1983; Winter 1989), and a surface comprising mixed $\text{U}^{\text{IV/V}}$ states has been shown to be catalytic for O_2 reduction (Hocking et al. 1991; Hocking et al. 1994), this change in composition can be expected to influence corrosion kinetics. The line A in Figure 9 shows that predicted (Shoesmith et al. 2003; Shoesmith et al. 1998) E_{CORR} values (over 10^6 years) fall within this range; i.e. the fuel surface should always be able to support corrosion. However, it should be noted this prediction does not take into account all the possible surface reactions, which could significantly reduce the value of E_{CORR} (section 10).

A number of additional features in Figure 8 are noteworthy.

- (i) Dissolution has been shown to commence as soon as the potential exceeds the threshold value of -0.4V (Rudnicki et al. 1994).
- (ii) For potentials greater than 0V (at room temperature; -0.2V at 60°C), a U^{VI} deposit begins to accumulate on the fuel surface. Since this deposit will be an insulator, it would be expected to block the fuel corrosion process occurring on the underlying conductive UO_{2+x} layer.

- (iii) At high potentials, the decrease in U^{VI} content of the surface indicates that passivation is incomplete. This can be attributed to the development of local acidity due to hydrolysis of dissolved U^{VI} (Wren et al. 2005),



At room temperature the onset of this process occurs around 0.3 to 0.35 V, Figure 8, while at 60°C, it can occur at a potential as low as 0.1 V (Broczkowski et al, 2007). The potential consequences of such a process will be further discussed below.

7. REACTIVITY OF THE FUEL SURFACE

Measurements of fuel corrosion rates show wide variations in fuel reactivity (Poinsot et al. 2005; Shoesmith et al. 1994; Oversby 1999). It is in some cases unclear whether these differences are attributable to real variations in fuel reactivity, or to differences in experimental conditions and specimen treatment. Reports of a difference between the measured dissolution currents for single crystals and sintered discs by a factor of 10^3 (Nicol et al. 1973), and between UO_2 and natural uraninites containing ill-defined impurities (Grandstaff et al. 1976), suggest that the presence of defects and impurities introduced during in-reactor fission (section 2) could exert a significant effect on the corrosion rate. Also, there is electrochemical evidence to show that fuel reactivity increases with the degree of non-stoichiometry (x in UO_{2+x}) (Shoesmith et al. 2001). While in-reactor irradiation is unlikely to lead to a significant change in the degree of non-stoichiometry, residual non-stoichiometry from the fuel fabrication process is likely to remain. The most likely location of this non-stoichiometry is within grain boundaries, making it difficult to know whether the grain boundary inventory of fission products is presently overconseratively included in the instant release fraction (section 2).

These features suggest that in-reactor burnup leading to lattice doping with fission products and the formation of noble metal epsilon particles could influence corrosion rates. Generally, it has been assumed that the primary influence of burnup will be to increase the instant release fraction and to enhance the radiation fields leading to the production of radiolytic oxidants (Johnson et al. 1994; Johnson et al. 1996; Tait et al. 2000; Garisto et al. 2004; Carbol et al. 2005). However, the increase in fission product doping of the UO_2 lattice has been shown to influence the kinetics of air oxidation of fuel (Thomas et al. 1993; Choi et al. 1996; Cobos et al. 1998; McEachern et al. 1998), leading to the suspicion that a similar influence on corrosion could be observed.

Raman spectroscopy studies show that fission product doping (varied in SIMFUELS (Lucuta et al. 1991; Matzke et al. 1991) with different degrees of simulated burnup) has a significant influence on the structure of UO_2 , Figure 12.

The peaks at $450cm^{-1}$ (P1) and $1150cm^{-1}$ (P2) are signatures for the well defined cubic fluorite lattice of UO_2 , and the broad peak(s) in the region $500-700cm^{-1}$ (P3) are attributed to a damaged lattice (He et al. 2007). The loss in intensity of P1 and P2 with respect to P3 as the fission product doping level increases clearly indicates a loss of cubic symmetry. This loss of symmetry correlates with an influence on the oxidation and dissolution currents, Figure 13. While the influence of doping (simulated burnup) on the oxidation step ($UO_2 \rightarrow UO_{2+x}$; $i_p^{(1)}$) is marginal there is a definite suppression in dissolution current ($UO_{2+x} \rightarrow UO_2^{2+}$; $i_p^{(2)}$) with increased doping.

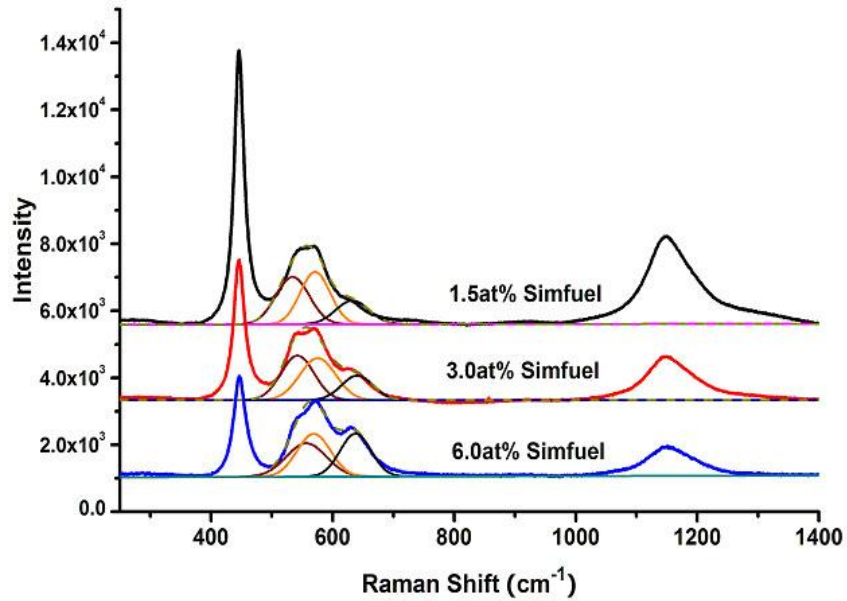


Figure 12: Raman spectra recorded on three SIMFUEL specimens with different degrees of simulated burnup (He et al. 2007).

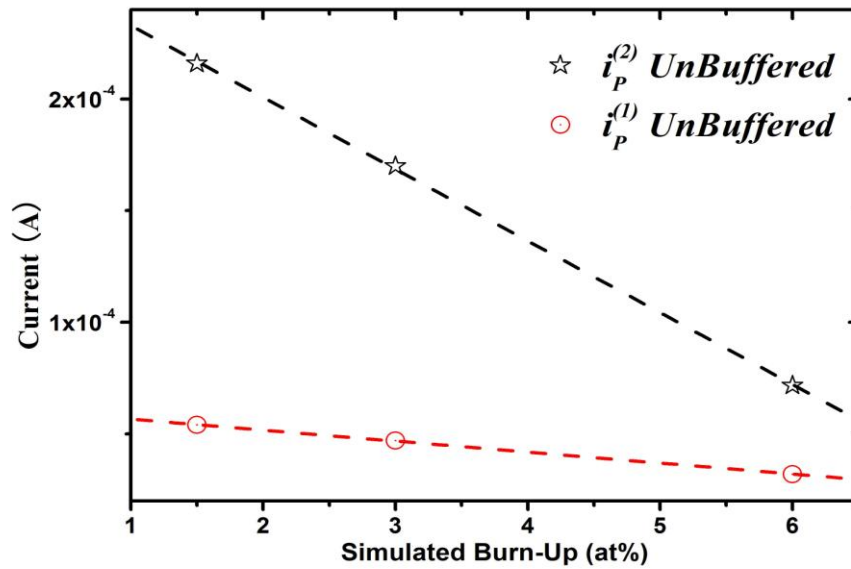


Figure 13: Anodic currents recorded on three SIMFUEL electrodes with different degrees of simulated burnup in 0.1 mol/L NaCl (pH=9.5): $i_p^{(1)}$ was recorded at a potential of + 0.1 V (vs. SCE) when only the surface oxidation reaction, $UO_2 \rightarrow UO_{2+x}$, is occurring: $i_p^{(2)}$ was recorded at +0.4 V (vs. SCE) when the predominant reaction occurring is the anodic dissolution reaction, $UO_{2+x} \rightarrow UO_2^{2+}$ (He et al. 2007).

This influence of fission product doping parallels that observed for air oxidation (Thomas et al. 1993; Choi et al. 1996; Cobos et al. 1998; McEachern et al. 1998). The reasons for this effect are not fully understood, but a possibility is that the formation of dopant-vacancy clusters reduces the availability of vacancy sites for O^{2-} incorporation into the surface, the first step in the oxidation/dissolution sequence. More pertinent is the evidence (from x-ray diffraction as well as Raman spectroscopy (He et al. 2007)) that doping to the 1.5 at % level exerts only a marginal effect on fuel reactivity. Since CANDU fuel burnups are commonly in this range (Johnson et al. 1994; Johnson et al. 1996; Garisto et al. 2004), any influence of burnup on the corrosion rate of CANDU fuel would be limited to its influence on cathodic kinetics (i.e., H_2O_2/O_2 reduction in support of fuel corrosion, section 9).

8. INFLUENCE OF CORROSION PRODUCT DEPOSITS

If fuel corrosion were to persist for long periods of time, then corrosion product deposits would accumulate on the corroding fuel surface. This accumulation could have a number of effects:

- 1) It would suppress corrosion by blocking the fuel surface to an extent determined by the porosity of the deposit, Figure 14.
- 2) It could restrict the diffusive mass transport of species to and from the reacting surface, Figure 14. Since the primary oxidant driving corrosion (H_2O_2) is produced by radiolysis at the fuel surface, a sufficiently thick, low porosity deposit could prevent diffusive loss of H_2O_2 from surface sites. Such a deposit could also hinder the access of redox scavengers (Fe^{2+} , H_2) to the corroding surface, thereby reducing the efficiency of scavenging.
- 3) Deposits could incorporate radionuclides released during fuel corrosion, thereby preventing, or at least delaying, their release to groundwater and modifying the yield and distribution of α -radiolysis products (Burns et al. 1997; Buck et al. 1998; Finch et al. 2002; Burns et al. 2004).
- 4) By restricting the diffusion of dissolved UO_2^{2+} away from the fuel surface, deposits could lead to a local acidification (via hydrolysis by reaction (2)) within pores in the deposit or within defects in the fuel surface (fractures, locations of missing grains, fission-induced porosity). In the absence of acidification, these pores and defects would be expected to seal by precipitation, since the concentration of dissolved U^{VI} would be highest at the fuel surface, and, hence, it is there that precipitation would most likely occur (if the concentration exceeds the solid solubility). However, the development of acidity at the fuel surface introduces a pH gradient within the pores/defects leading to an inverse gradient in solubility, which could maintain porosity and sustain film growth, as illustrated schematically in Figure 15.

8.1 Influence of Redox Conditions and Groundwater Speciation on the Nature of Surface Deposits

The physical and chemical properties of deposits will be determined by the combination of redox conditions, temperature, and groundwater composition. The key groundwater constituents are $\text{CO}_3^{2-}/\text{HCO}_3^-$, which will increase UO_2^{2+} solubility and hinder the formation of deposits, and Ca^{2+} and silicate, which will stabilize insoluble UO_2^{2+} deposits. As discussed above in section 3, the groundwater entering the failed container could contain both HCO_3^{2-} and Ca^{2+} .

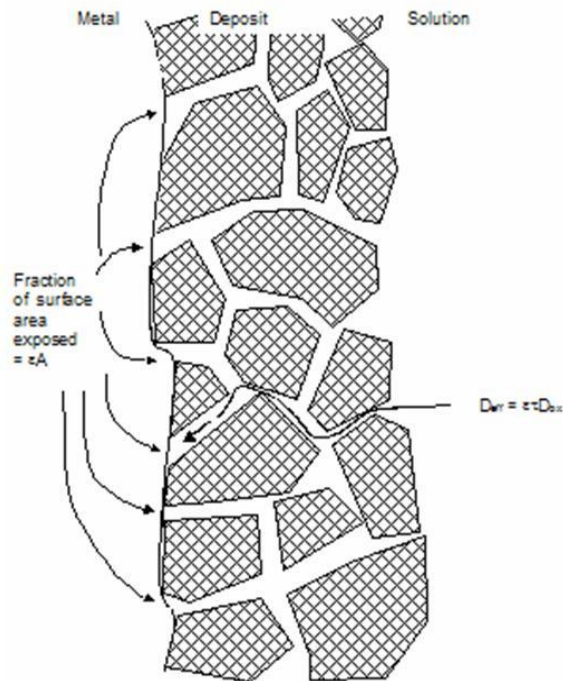


Figure 14: Illustration showing a porous deposit on a corroding surface exposed to an aqueous environment. The presence of the deposit leads to a decrease in the area of the corroding surface (A) exposed to the solution, and to a slowing of the diffusion of solution soluble species to the surface: D_{ox} is the diffusion coefficient of the soluble species; ϵ is the porosity of the deposit, τ is the tortuosity of the pores, and D_{eff} is the effective diffusion coefficient of the soluble species ($D_{eff} = \epsilon\tau D_{ox}$).

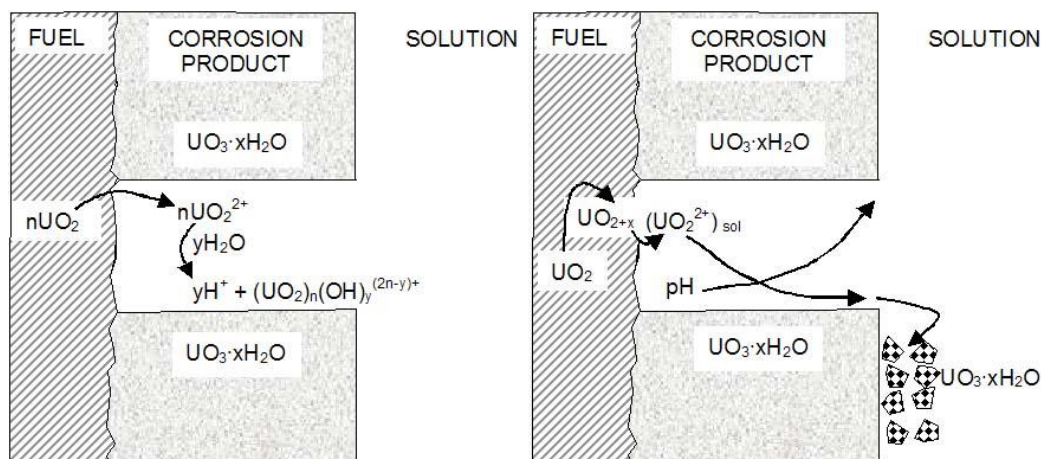


Figure 15: Illustrations showing the influence of a corrosion product deposit on the local chemistry at the corroding fuel surface. The first panel shows that the hydrolysis of dissolved U^{VI} (UO₂²⁺) at the fuel surface produces a lower pH at the corroding surface than at the mouth of the pore. As illustrated in the second panel, this pH gradient leads to a solubility gradient within the pore. Since the solubility is highest at the corroding surface, dissolved UO₂²⁺ diffuses down the solubility gradient and deposits (as UO₃·xH₂O) on the outside of the deposit.

The influence of deposits is hard to study on a laboratory timeframe since their rate of accumulation is very slow, especially when redox conditions are only slightly oxidizing. However, similarities in the alteration phases (redeposited dissolved U solids) observed in laboratory experiments and those observed in the geological alteration of natural uraninite deposits (Buck et al. 1997; Wronkiewicz et al. 1996; Wronkiewicz et al. 1992; Finch et al. 1999; Office of Civilian Radioactive Waste Management 2004) provides evidence that the overall alteration processes observed in the laboratory are similar to those likely to control alteration over the repository time frame (Finch et al. 1992; Finch et al. 1991).

Most studies on the influence of Ca²⁺ and silicate on the formation of surface deposits have been performed under oxidizing conditions, and clearly demonstrate the incorporation of these species into oxidized uranium phases. Consequently, U^{VI} silicates are expected to be the primary, thermodynamically stable phases formed by fuel alteration under Yucca Mountain (Nevada, USA) conditions (Office of Civilian Radioactive Waste Management 2004). In addition, single-pass flow-through loop experiments and electrochemical studies show that the effect of these two species is immediate (after their addition), suggesting a direct effect on the kinetics of the dissolution process as well as on the nature of the deposits formed. Uranium concentrations measured in the flow-through loop experiments with UO₂ pellet fragments showed the fuel corrosion rates and radionuclide release rates to be suppressed by a factor of 200, with the larger influence being exerted by the silicate (up to a factor of 100) (Wilson et al. 1990; Tait et al. 1997).

Figure 16 shows that the replacement of Na⁺ by Ca²⁺ in a 0.1 mol/L chloride solution very significantly suppresses the anodic dissolution of UO₂ at 0.25 V, a strongly oxidizing potential (Figures 8 and 9). Experiments at less oxidizing potentials (0.1 V) showed that Ca²⁺ did not inhibit the initial surface oxidation step (UO₂ → UO_{2+x}), Figure 17, confirming that its influence is primarily on the dissolution step (UO_{2+x} → UO₂²⁺). Since there was no evidence for its

incorporation into surface phases in these short term experiments, the influence of Ca^{2+} was attributed to its ability to absorb on the fuel surface and retard protonation steps involved in dissolution (Santos et al. 2006a).

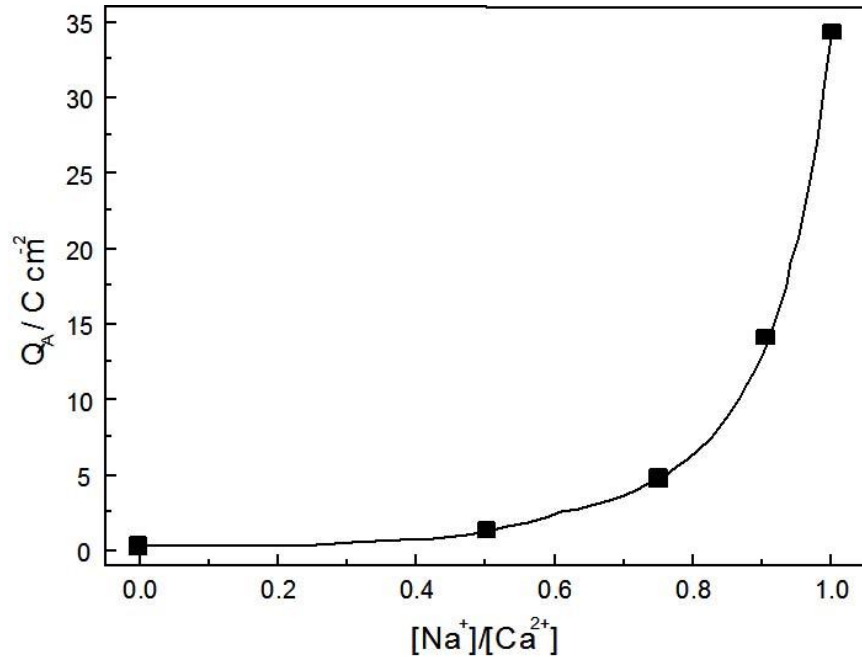


Figure 16: Anodic dissolution charges measured on a 1.5wt% SIMFUEL in a 0.1 mol/L solution (pH = 9.5) containing different ratios of CaCl_2 and NaCl . The charges were measured after 100 hours of anodic oxidation at 0.25 V, and are directly proportional to the number of moles of dissolved U, which could be calculated using Faraday's Law (Santos et al. 2006a).

Silicate also suppresses the anodic dissolution of UO_2 (Santos et al. 2006b), but by incorporation into U^{VI} deposits which form on the fuel surface, Figure 18 (A and B). The coadsorption of water indicates that dissolution is suppressed by the accumulation of a hydrated U^{VI} silicate deposit. More recent experiments conducted at low applied dissolution currents confirm the formation of a U^{VI} silicate deposit, Figure 19.

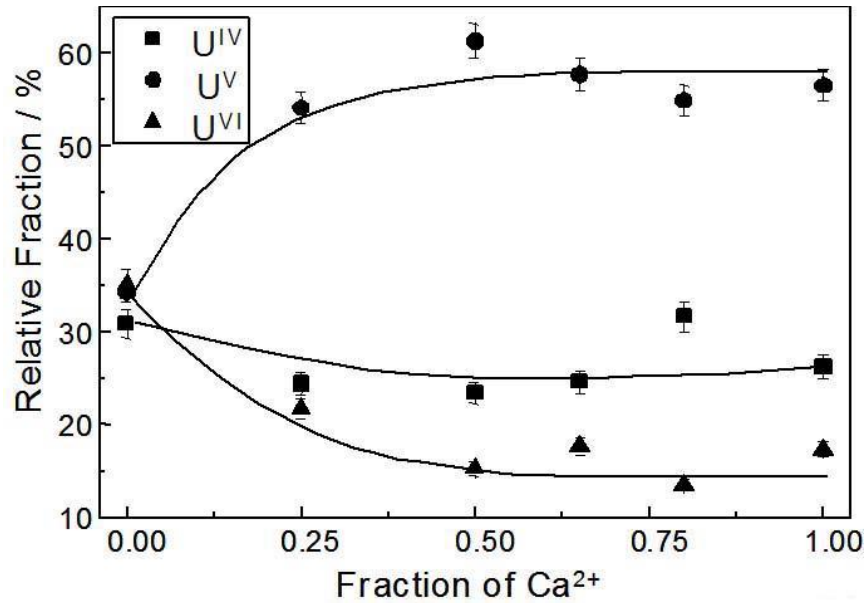


Figure 17: The relative fractions of the three uranium oxidation states in the surface of a 1.5wt% SIMFUEL electrode as a function of the fraction of Ca²⁺ present in a NaCl/CaCl₂ solution with an overall concentration of 0.1 mol/L (pH = 9.5). Each anodic oxidation was performed at 0.1 V for 18 hours prior to surface analysis by XPS. The dominance of the U^V state confirms that the oxidation reaction (UO₂ → UO_{2+x}) is not retarded in a Ca²⁺- dominated solution (Santos et al. 2006b).

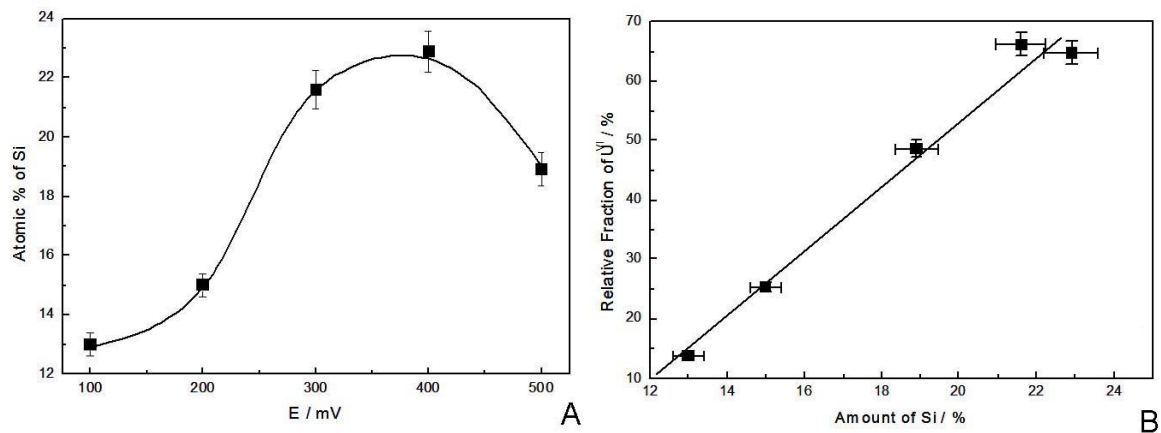


Figure 18: A - Atomic percentage of Si on the surface of an electrochemically-oxidized 1.5wt% SIMFUEL electrode. B- Correlation between the amounts of U^{VI} and silicate on the SIMFUEL surface. The electrode was anodically oxidized at each potential for 1 hour in a solution containing 0.1mol/L silicate + 0.1mol/L NaCl (pH = 9.5) prior to surface analysis by XPS. B shows that the amounts of U^{VI} and silicate on the electrode surface are correlated, indicating the formation of a U^{VI} silicate surface deposit (Santos et al. 2006b).

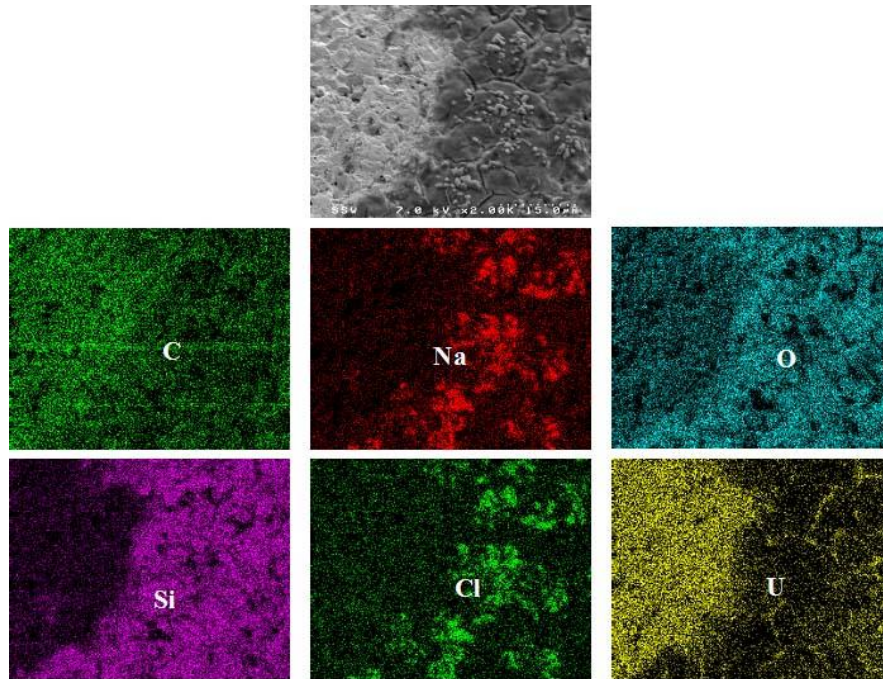


Figure 19: Scanning electron microscopy (SEM) image and energy dispersive X-ray (EDS) maps of a 1.5 wt% SIMFUEL surface slowly electrochemically oxidized in a solution containing 0.1 mol/L NaSiO_3 + 0.1 mol/L NaCl (pH = 9.5). A current of 20 nA was applied for 600 hours prior to analysis of the surface. The SEM image shows an area of the surface covered by deposit (right hand side) and an uncovered area (left hand side). The strong Si and O, and lower U, signals indicate the deposit is a U^{VI} silicate. The localized signals for Na and Cl can be attributed to the presence of NaCl in the wet porous deposit when the electrode is in the electrochemical cell. When the specimen is removed and placed in the microscope, the water evaporates leaving behind the NaCl.

For the initially slightly oxidizing to long-term anoxic conditions expected in a deep geologic repository, the investigation of the influence of corrosion product films is considerably more difficult. Attempts to analyze deposits (alteration products) on the surface of fuel specimens exposed to solutions containing Ca^{2+} and silicate were unsuccessful, although the formation of coffinite ($\text{USiO}_4 \cdot n\text{H}_2\text{O}$) was suspected, and minor amounts of ekanite may have been formed (Amme et al. 2005). However, the presence of silicate clearly suppressed dissolved U concentrations, suggesting a direct influence on the chemical dissolution process. While by themselves inconclusive, these observations are consistent with analyses from the Cigar Lake deposit (Saskatchewan, Canada) where reducing conditions were maintained by the presence of pyrite oxidation to yield the redox scavenger, Fe^{2+} . Analyses of samples from this deposit showed no evidence for the formation of oxidized secondary deposits, and only very minor evidence for chemical conversion to coffinite (Cramer et al. 1994). The mixed $\text{U}^{\text{IV/VI}}$ solid, ianthinite, has been observed under oxidizing conditions (Burns et al. 1997), but the authors speculated that its formation was a consequence of local depletions of oxidants at the sites at which it was observed.

Figure 20 summarizes the phases that would be anticipated to form under different redox conditions based on published studies. The mineralogy of U is very complex (Wronkiewicz 1999), and the phases given represent general observations and not an exhaustive list of possibilities.

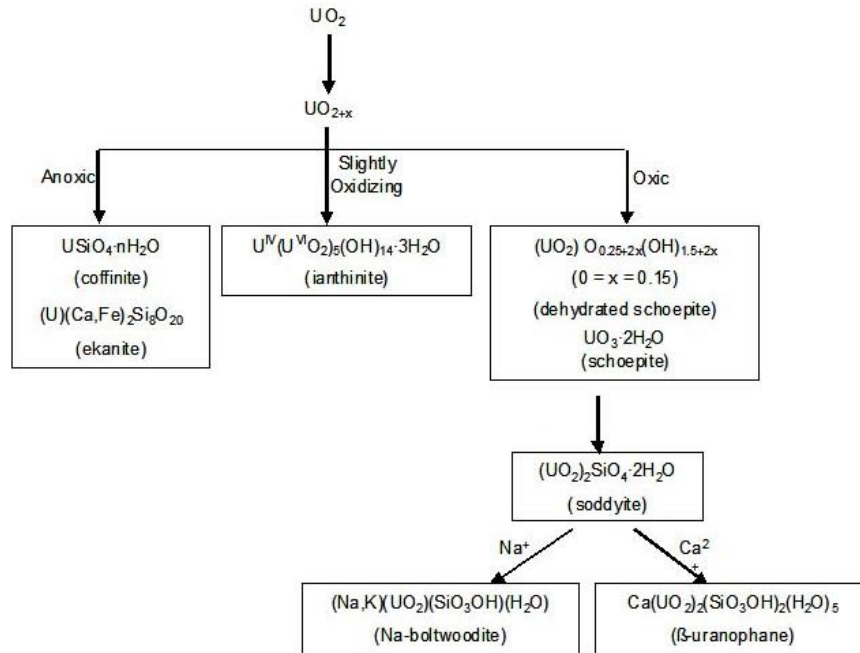


Figure 20: Possible secondary phases that could form under different redox conditions on a corroding/ dissolving UO_2 surface.

While these studies identify the chemical nature of phases that may form as deposits on UO_2 , they provide no information on the physical properties of deposits required to determine their behaviour on the fuel dissolution/corrosion process. Of particular importance is their porosity since this parameter will have a significant effect on the chemical conditions at the fuel surface. In particular, its influence on diffusive mass transfer of species to and from surface active sites will be the primary determinant of surface redox conditions and their control by redox active species in the groundwater, in particular the products of steel corrosion (Fe^{2+} and H_2). These difficulties make it necessary to make assumptions when attempting to model the influences of deposits (Shoesmith et al. 2003), and then attempt to test the assumptions by comparing the model predictions with observations.

8.2 Development of Local Acidity at the Corroding Fuel Surface

The possibility of forming acidic conditions within surface flaws in the fuel and/or pores in corrosion product deposits has been identified in electrochemical experiments (Santos et al. 2004; Santos et al. 2006c) and in corrosion experiments with used fuel (Shoesmith et al. 1996). It is also suspected to occur at high alpha dose rates (Wren et al. 2005), and is the most likely explanation for the aggressive corrosion observed on spent fuel specimens tested in unsaturated drip tests (Finn et al. 1994; Finn et al. 1997). Electrochemical studies (Santos et

al. 2006) have shown that the mechanism of oxidation/dissolution of fuel changes for $\text{pH} \leq 5$. Oxidation of the surface to UO_{2+x} prior to dissolution is no longer observed and both the solubility (Grenthe et al. 1992) and the dissolution rate (in aerated solutions (Torrero et al. 1997)) increase substantially.

In Figure 9, acidification is identified as a possibility for potentials above about 0.1 V, but electrochemical experiments indicate that the process cannot be ruled out for potentials as low as 0 V (Santos et al. 2006). Model calculations (Shoesmith et al. 2003) indicate that the maximum E_{CORR} sustainable at expected alpha dose rates could approach about -0.05 V (line A in Figure 9) introducing the possibility that local acidification may be possible.

Under natural corrosion conditions anodes and cathodes are not artificially separated as they are in an electrochemical experiment, and the alkalinity produced by oxidant reduction ($\text{H}_2\text{O}_2 + 2\text{e}^- \rightarrow 2\text{OH}^-$) should, at least partially, neutralize the acidity produced by the anodic reaction, as illustrated in Figure 21. However, separation of anodes and cathodes can be achieved if the surface properties are non-homogeneous, as they will be in used fuel due to the presence of grain boundaries, which may differ from grains in composition, and noble metal epsilon particles (section 2). If container failure were to occur early, while γ/β radiation fields were significant, experiments on used fuel indicate that the development of acidity would be a real possibility (Shoesmith et al. 1996). However, for the low alpha dose rates expected if container failure were delayed, it is experimentally very difficult to determine whether local acidification is possible or not, and attempts to model the process are underway (Cheong et al. 2007). The primary goal of such a model is to determine whether the conditions required to produce acidity are achievable at the slow rates of fuel corrosion anticipated within a failed container.

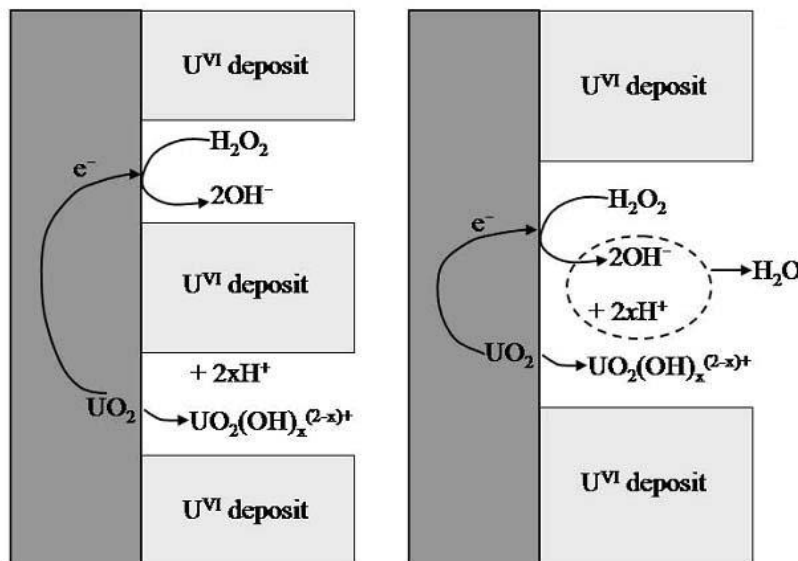


Figure 21: Illustrations showing how acidity can develop within pores in a corrosion product deposit. The first panel shows that acidity can develop at the anodic dissolution site providing it is separated spatially from the cathodic site. The second panel shows that, if the two sites are not separated, then the alkalinity produced by H_2O_2 reduction will, at least partially, neutralize the acidity.

The reactions considered, and the model format used, for the anodic dissolution reaction (assuming the cathodic reaction occurs at a remote galvanically-coupled site) are illustrated in Figure 22. The ability to develop acidity will be related to the relative rates of fuel dissolution at the base of pores (or flaws) and the diffusive flux of protons away from the fuel surface to the bulk of solution. The fuel dissolution rate is related to the redox conditions (E_{CORR} at the fuel surface) and the dimensions of the pore/flaw (i.e., its depth and cross sectional area). The additional influences of groundwater species (Ca^{2+} , silicates, HCO_3^-/CO_3^{2-}) which could diffuse into the pore have, so far, not been considered.

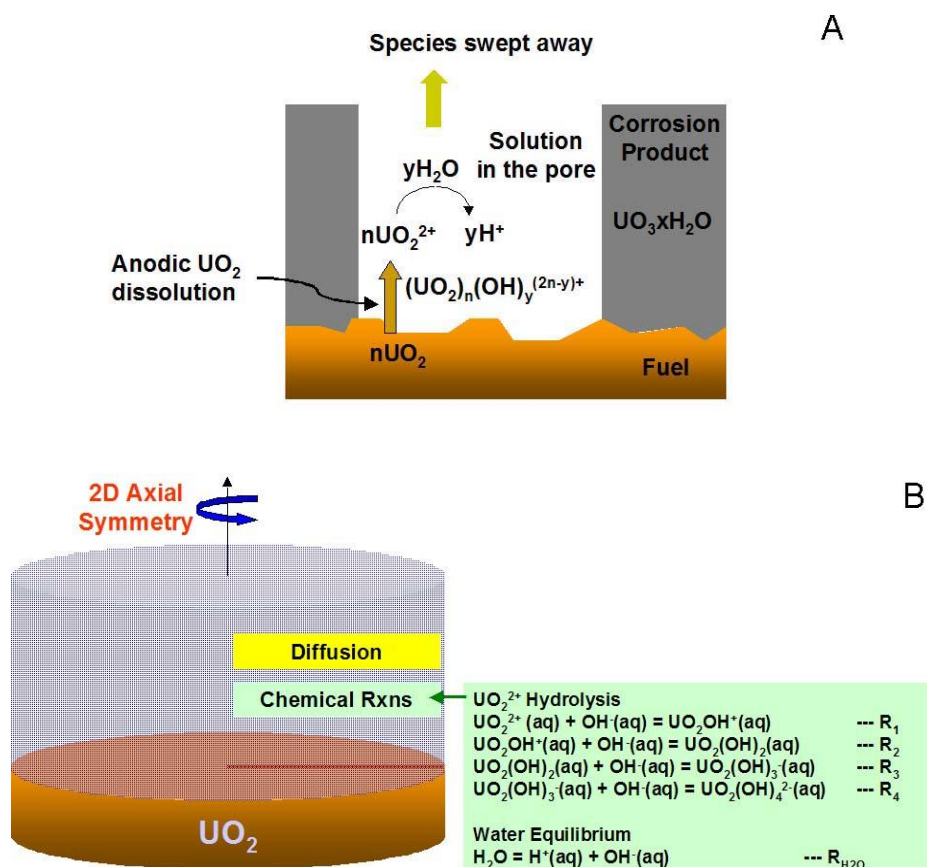


Figure 22: A - Illustration showing the electrochemical, chemical, and transport processes considered in a model to predict the pH at the bottom of a pore in a corrosion product ($UO_3 \cdot xH_2O$) deposit on a corroding UO_2 surface.

B - Illustration showing the axial symmetry assumed for the pore, and the hydrolysis reactions involved in generating acidity (Cheong et al. 2007).

Preliminary calculations, Figure 23, show that, as demonstrated experimentally, Figures 8 and 9, acidity can develop in relatively shallow pores/flaws ($\sim 1\mu m$ deep) at oxidizing potentials (0.3 V), but a pore/flaw approaching 1 mm in depth would be required for this to happen at -0.05 V, the maximum potential thought sustainable by alpha radiolysis (line A in Figure 9).

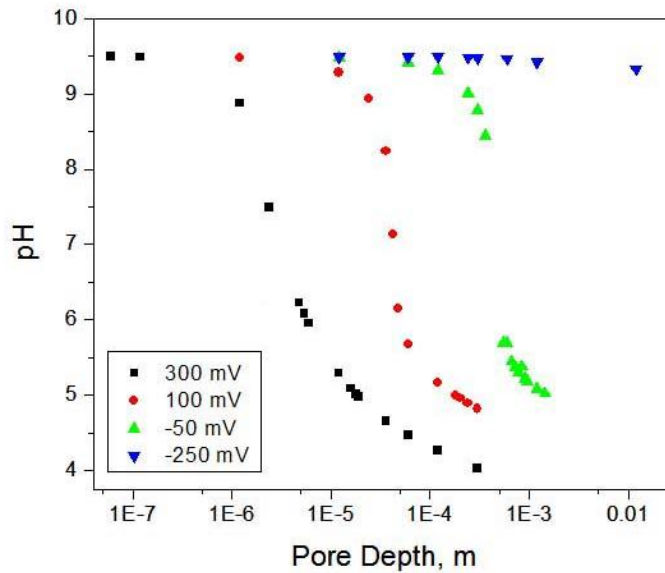


Figure 23: The pH predicted at the base of a pore in a corrosion product deposit as a function of pore depth and the potential at which dissolution was occurring. The anodic dissolution reaction rate increases exponentially with applied potential (Cheong et al. 2007).

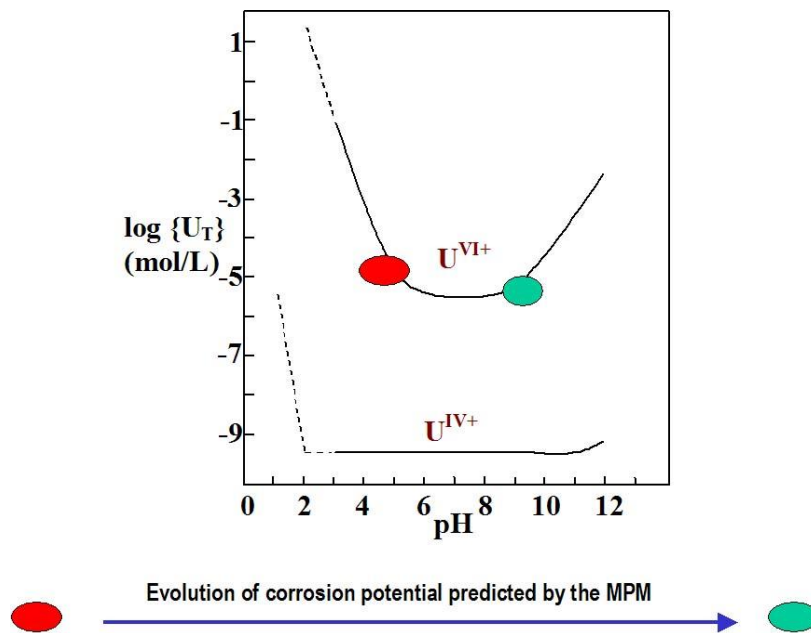


Figure 24: The influence of the maximum pH change predicted at the base of a 300 μ m deep pore on UO_2 dissolution occurring at a potential of 300mV. The calculated values are superimposed on plots of the solubility of U^{IV} and U^{VI} taken from Grenthe et al. (1992).

For a potential of -0.25 V (the minimum predicted potential, ignoring any influence of hydrogen), for acidity development appears impossible since pores/flaws > 1 cm in depth would be required. In addition, the pH at the base of a pore for a potential of -0.05 V would be less than 5. Such pH depression would have only a minor influence on solubility, Figure 24, but significant influence on corrosion rate, Figure 25. While further studies, especially on the influence of temperature, are required, these calculations clearly indicate that the influence of local acidity should exert only a marginal effect on fuel corrosion behaviour.

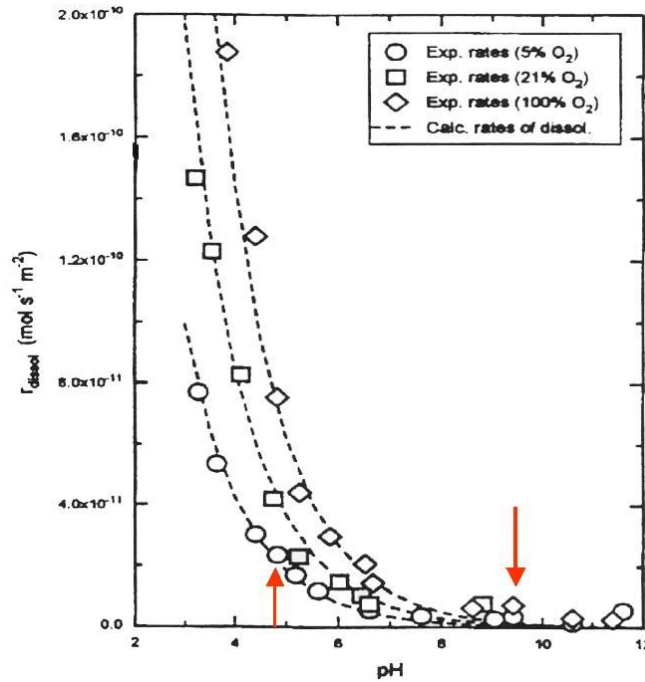


Figure 25: Measured dissolution rates of UO_2 as a function of pH in a 0.1 mol/L NaClO_4 solution purged with gas containing various percentages of O_2 [Torrero et al. 1997]. The arrow at pH = 9.5 indicates the assumed bulk solution pH in the model described in Figure 22. The arrow at pH=4.8 shows the minimum predicted pH at a potential of 0.3 V (vs. Ag/AgCl) for a 300 μm deep pore in a corrosion product deposit on the fuel surface (from Figure 23).

8.3 The Influence of Carbonate on Fuel Corrosion

While Ca^{2+} and silicate are the species most likely to promote the formation of deposits, the groundwater species most likely to prevent it are $\text{HCO}_3^-/\text{CO}_3^{2-}$. Carbonate is a strong complexing agent for the uranyl ion (UO_2^{2+}) (Grenthe et al. 1992; Shoesmith et al. 1994), which leads to a considerable increase in this ion's solubility, and an acceleration of fuel corrosion (Shoesmith et al. 2003; Shoesmith et al. 1984; Shoesmith et al. 1983; de Pablo et al. 1996; Hossain et al. 2006; Goldik et al. 2006; Luht 1998; Stroes-Gascoyne et al. 2005; Sunder et al. 1992; de Pablo et al. 1999; Ilin et al. 2001; Cobos et al. 2003),



Both electrochemical (Shoesmith 2000; Shoesmith et al. 2003; Shoesmith et al. 1984; Shoesmith et al. 1983) and chemical studies (de Pablo et al. 1996; Hossain et al. 2006; de Pablo et al. 1999; Ilin et al. 2001; Cobos et al; 2003) yield consistent results. When the total $\text{HCO}_3^-/\text{CO}_3^{2-}$ concentration is $\geq 10^{-3}$ mol/L, which is possible under anticipated groundwater conditions (section 3), formation of U^{VI} deposits is prevented, and oxidative dissolution proceeds uninhibited at a rate 2 to 3 orders of magnitude greater than in the absence of carbonate. As the carbonate concentration is increased, $\text{HCO}_3^-/\text{CO}_3^{2-}$ not only prevents deposition, but inhibits formation of the underlying UO_{2+x} layer (de Pablo et al. 1996; Hossain et al;) and catalyzes fuel dissolution via a surface complexation process (Goldik et al. 2006).

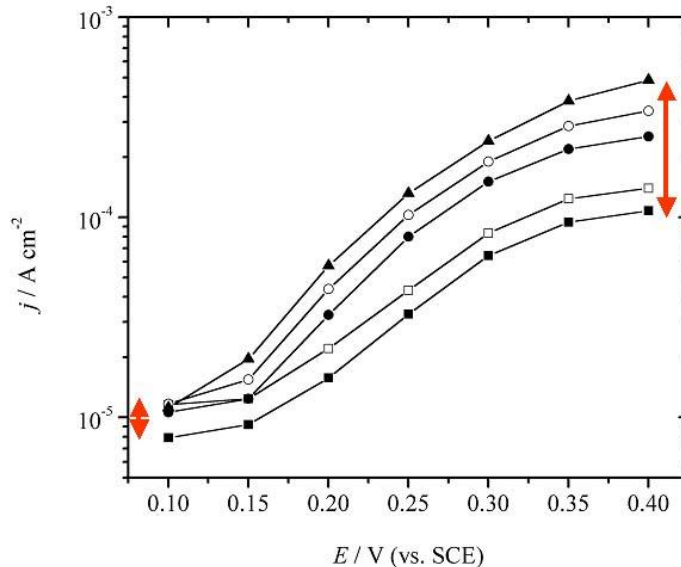
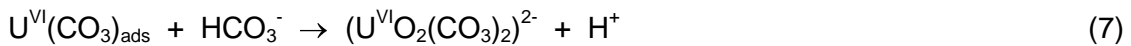
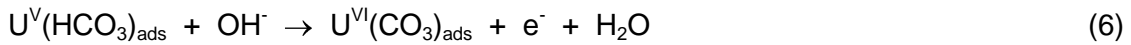


Figure 26: Steady-state electrochemical dissolution currents measured on a 1.5wt% SIMFUEL electrode as a function of applied potential in a 0.1 mol/L NaCl solution (pH=9.7) containing various concentrations of $\text{HCO}_3^-/\text{CO}_3^{2-}$: (■) 5×10^{-3} mol/L; (□) 10^{-2} mol/L; (●) 5×10^{-2} mol/L; (○) 10^{-1} mol/L; (▲) 2×10^{-1} mol/L [Goldik 2006]. At positive potentials (strongly oxidizing conditions) the levelling off of the current indicates dissolution is becoming independent of potential. The arrow at the high potential limit indicates the dissolution reaction is dependent on total carbonate concentration under strongly oxidizing conditions. The levelling off of the current and the arrow at the low potential limit shows that the reaction is becoming independent of both potential and total carbonate concentration under weakly oxidizing conditions.

The influence of carbonate on the kinetics of fuel dissolution decreases with decreasing concentration and potential. As the concentration decreases below 10^{-4} mol/L, any influence on dissolution becomes negligible (Hossain et al. 2006) and corrosion product deposition becomes possible at oxidizing potentials. Electrochemical studies show that, irrespective of concentration, the influence of carbonate disappears as the potential is reduced, and consequently less oxidizing, Figure 26. Thus, as radiation fields decay, and redox conditions become less oxidizing, any acceleration of fuel corrosion by HCO_3^{2-} will disappear.

9. KINETICS OF REDUCTION OF CATHODIC REAGENTS

As shown in Figure 6, the overall corrosion reaction is composed of two half reactions; the anodic dissolution of fuel, and the cathodic reduction of radiolytic oxidants, including the radical species OH^\bullet , HO_2^\bullet , $\text{CO}_3^{\bullet-}$ (in carbonate solutions), Cl^\bullet (in chloride) and the molecular oxidants, H_2O_2 and O_2 . The corrosion rate will be controlled by whichever of these two half reactions is kinetically the slowest. Consequently, considerable effort has been expended in determining the mechanism and kinetics of possible cathodic reactions, since they could control both the rate and overall extent of fuel corrosion.

If container failure occurs while γ/β radiation fields are significant, fuel corrosion will be driven by both radical and molecular oxidants (Shoesmith 2000; Shoesmith et al. 1996; Sunder et al. 1992; Shoesmith et al. 1992). However, while the rate constants for the reaction of radiolytic radicals with the fuel surface have been shown to be large (Ekeroth et al. 2003), the steady-state radical concentrations are low and fuel corrosion is dominated by reaction with H_2O_2 , which is present in substantially larger amounts. If container failure is delayed until γ/β fields are insignificant (> 500 to 1000 years, Figure 7) and only the α -radiolysis of water is important, H_2O_2 would be expected to totally dominate radiolytic corrosion. However, H_2O_2 decomposition could produce the additional oxidant, O_2 ($2\text{H}_2\text{O}_2 \rightarrow 2\text{H}_2\text{O} + \text{O}_2$), which has been shown to react ~ 200 times slower with the fuel surface than does H_2O_2 (Shoesmith 2000; Wren et al. 2005; Shoesmith et al. 1989), and fuel corrosion could be correspondingly significantly slower.

9.1 Kinetics of Oxygen Reduction

The cathodic reduction of O_2 is notoriously slow due to the need to break the strong O-O bond (Hocking et al. 1991). On oxide surfaces this reaction is catalyzed by mixed oxidation states (termed donor-acceptor sites) in the oxide surface. On UO_{2+x} these sites are adjacent $\text{U}^{\text{IV}}/\text{U}^{\text{V}}$ atoms which relay electrons released by the anodic fuel oxidation/dissolution reaction to O_2 molecules adsorbed on the oxide surface, as illustrated schematically in Figure 27A. The rate of O_2 reduction is controlled by the transfer of the first electron (in the sequence of four required for total reduction; $\text{O}_2 + 2\text{H}_2\text{O} + 4\text{e}^- \rightarrow 4\text{OH}^-$) (Hocking et al. 1991; Hocking et al. 1994).

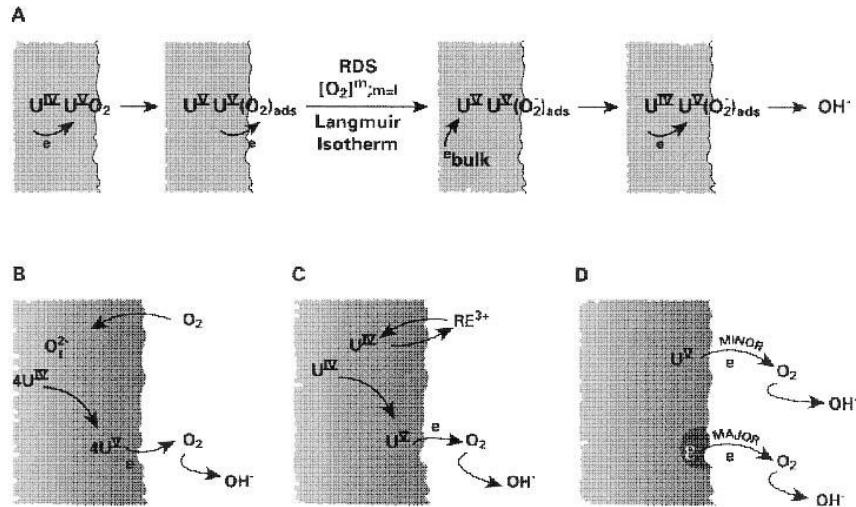


Figure 27: Schematic illustrations indicating the influence of various factors on O_2 reduction on UO_2 surfaces (Shoesmith 2000).

A - Illustrates the occurrence of O_2 reduction at donor-acceptor sites (U^{IV}/U^V adjacent atoms) in the UO_2 surface. The rate-determining step (RDS) is the transfer of the first electron in the sequence of four, and is first order in O_2 concentration. Since the donor-acceptor sites are widely distributed, the reaction occurs under Langmuir isotherm conditions.

B - Oxidation of the fuel surface catalyzes O_2 reduction by incorporation of O^{2-} at interstitial sites in the UO_2 lattice leading to the creation of additional donor-acceptor surface sites.

C - In-reactor fission creates rare-earth (RE^{3+}) dopants at uranium lattice sites, leading to the creation of additional donor-acceptor sites, which could catalyze O_2 reduction.

D - In-reactor fission creates noble metal epsilon (ϵ) particles, which catalyze O_2 reduction.

As illustrated in Figure 8, such a catalytic surface will exist once the potential is above the threshold of $-0.4V$ required for fuel corrosion to occur. Natural corrosion experiments in aerated solutions confirm that an increase in the number density of donor-acceptor sites ($UO_2 + x/2O_2 \rightarrow UO_{2+x}$) does occur, leading to a corresponding increase in O_2 reduction current, Figure 27B (Hocking et al. 1991; Hocking et al. 1994; Betteridge et al. 1997) in electrochemical experiments. Attempts to further increase the rate of O_2 reduction by electrochemical oxidation actually lead to a decrease in O_2 reduction current due to the blockage of U^{IV}/U^V donor-acceptor sites by insulating U^{VI} species ($UO_{3 \cdot y}H_2O$) (Betteridge et al. 1997).

Inspection of Figures 8 and 9 shows coverage by U^{VI} occurs once the potential exceeds 0 to 0.1 V, and experimental measurements in aerated solutions confirm that E_{CORR} resides in this potential range (Shoesmith et al. 1989). For lower O_2 concentrations, E_{CORR} is $< 0 V$ and corrosion, while slower, will be sustainable on the UO_{2+x} surface and not inhibited by the rate of release of U^{VI} species from the fuel surface. Thus, as the O_2 concentration decreases, kinetic control of the corrosion reaction will switch from the anodic reaction to the cathodic reaction. When O_2 concentrations are high, release of U^{VI} species, formed by the anodic oxidation of the fuel surface, will be rate-controlling, while at low O_2 concentration the reduction of O_2 on the limited number of available donor-acceptor sites will be the slowest reaction step. Given the low oxidant concentrations anticipated under repository conditions, cathodic control of the

overall corrosion reaction would be expected if O_2 (formed from H_2O_2 decomposition) was the primary oxidant.

Two possible effects of in-reactor burnup on O_2 reduction can be identified; (i) fission product doping with rare earth (RE^{III}) ions which will increase the number density of U^{IV}/U^V donor-acceptor sites, Figure 27C; and (ii), the creation of epsilon particles which contain the noble metals Ru, Rh, and Pd, all of which have been shown to catalyze O_2 reduction (Anastasijevic et al. 1986; Vracar et al. 1986; Vracar et al. 1987; Martinovic et al. 1988; Kim et al. 1995; Kubatko et al. 2003).

Rare earth doping alone has only a marginal effect on the kinetics of O_2 reduction, but an increase in number and size of epsilon particles (over the simulated burnup range 1.5 at% to 6 at%) systematically increases the rate of O_2 reduction, Figure 28. Thus, O_2 reduction in support of fuel corrosion would occur preferentially on epsilon particles rather than on the UO_2 surface, Figure 27D. This would mean that the separation of anodes and cathodes, required for the generation of local acidity at anodic sites (section 8), could occur.

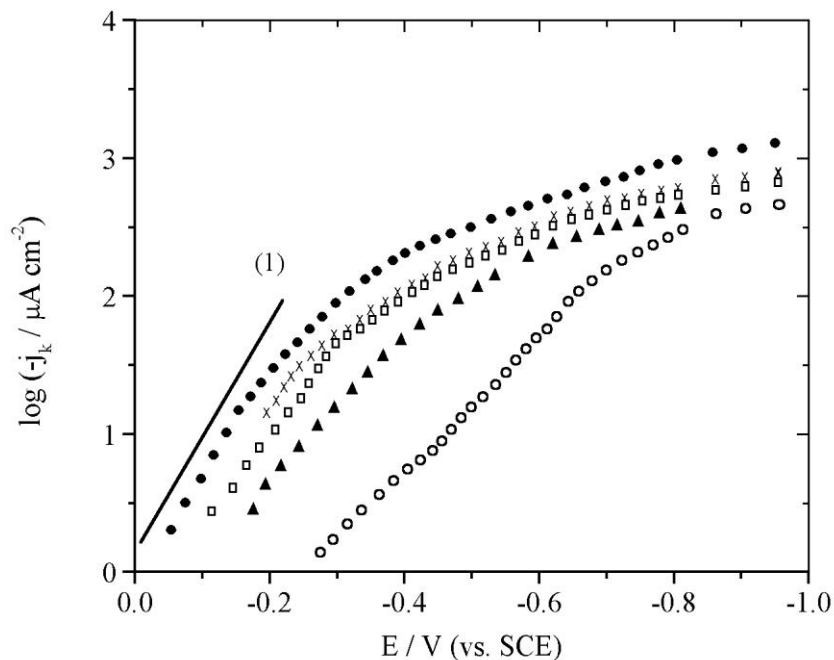


Figure 28: O_2 reduction currents recorded on various SIMFUEL electrodes in a 0.1 mol/L NaCl (pH=9.5) solution purged with air ($[O_2]=2.5 \times 10^{-4}$ mol/L): (o) fission product-doped UO_2 containing no epsilon particles; (▲) 1.5wt% SIMFUEL; (□) 3wt% SIMFUEL; (●) 6 wt% SIMFUEL; (x) 3wt% SIMFUEL containing epsilon particles but no fission-products. The current increases as the number and size of the epsilon particles in the UO_2 increases. In the absence of epsilon particles the current is significantly lower. The presence of epsilon particles in the absence of dopants gives high currents confirming that O_2 reduction is catalyzed on the particles, and not on the doped UO_2 surface. The line (1) is drawn with a slope of 90 mV/decade of current, the slope expected on noble metals. For the 6wt% SIMFUEL, the log current-potential relationship achieves this slope at low potentials, demonstrating the catalytic effect of the epsilon particles.

9.2 Kinetics of Hydrogen Peroxide Reduction

The cathodic reduction of H_2O_2 is considerably faster (200 times) than that of O_2 (Shoesmith 2000; Shoesmith et al. 1998) and its effect on UO_2 corrosion has been extensively studied (Sunder et al. 2004; Gimenez et al. 1996; de Pablo et al. 1996; de Pablo et al. 2001; Corbel et al. 2006; Wren et al. 2005; Hossain et al. 2006; Eary et al. 1983; Brown 1980; Diaz-Arocas et al. 1995; Amme 2002; Amme et al. 2002; Hiskey 1980; Christensen et al. 1990; Jonsson et al. 2004; Goldik et al. 2004; Goldik et al. 2005; Goldik et al. 2006a, Goldik et al. 2006b). This higher rate can be attributed to the ability of H_2O_2 to create its own $\text{U}^{\text{IV}}/\text{U}^{\text{V}}$ donor-acceptor sites,



rather than rely on the number of such sites pre-existing in the fuel surface, as is the case with O_2 reduction. This site is subsequently reduced by the electrons liberated by the anodic dissolution reaction,



The creation of donor-acceptor sites in this manner would also be expected to catalyze peroxide decomposition, as illustrated schematically in Figure 29. Consequently, under natural corrosion conditions, H_2O_2 would be expected to not only oxidize the UO_2 surface but to catalyze its own decomposition, and claims that decomposition occurs have been advanced (Diaz-Arocas et al. 1995; Amme 2002; Amme et al. 2002; Hiskey 1980).

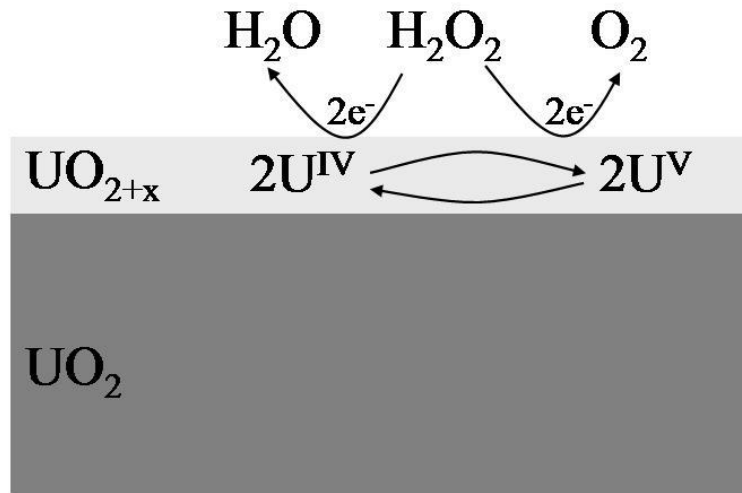


Figure 29: Illustration showing the H_2O_2 decomposition reaction catalyzed on a non-stoichiometric UO_{2+x} surface.

However, as observed for O_2 reduction, corrosion and decomposition are blocked at sufficiently high H_2O_2 concentrations ($\geq 10^{-4}$ mol/L) by the formation of U^{VI} surface species. These states

block the surface and retard regeneration of the catalytic (UO_{2+x}) surface, required for reaction 8. This means that, for sufficiently high H_2O_2 concentrations, corrosion is limited by the rate of release of U^{VI} species from the blocked surface, i.e., by the same limiting reaction observed for corrosion in O_2 solutions. This claim is confirmed by the similar E_{CORR} values measured in the presence of either oxidant (Sunder et al. 2004). An attempt to illustrate this mechanism is shown in Figure 30.

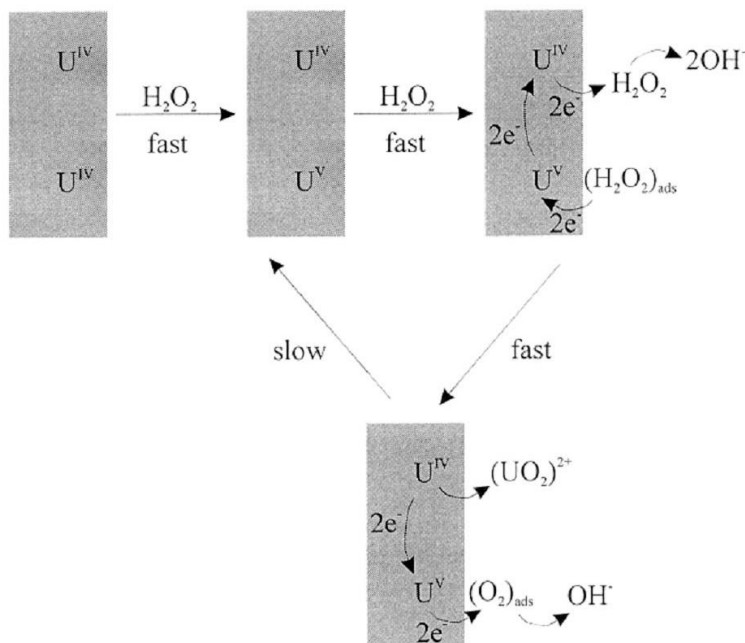


Figure 30: Illustration showing how H_2O_2 decomposition is blocked on an oxidized UO_2 surface. The mechanism shows that UO_2 is oxidized by H_2O_2 in two fast steps to a non-stoichiometric surface that could sustain H_2O_2 decomposition. However, the surface becomes blocked by adsorbed O_2 and U^{VI} (UO_2^{2+}) species, and the slow consumption of O_2 and release of UO_2^{2+} to solution is required to regenerate the non-stoichiometric surface required to sustain decomposition. As a consequence, decomposition can proceed no faster than the fuel corrosion reaction.

These data show that the mechanism of cathodic reduction of H_2O_2 and O_2 proceed via the same basic sequence of reactions. The faster kinetics for H_2O_2 reduction compared to those for O_2 reduction mean that the transition from anodic control of the fuel process, by the release of U^{VI} from the surface, to cathodic control by H_2O_2 reduction will not occur as readily for H_2O_2 as it does for O_2 reduction. This is confirmed by measurements that show E_{CORR} can still achieve values greater than 0V for concentrations as low as 10^{-5} mol/L H_2O_2 .

However, model calculations based on available data (Shoesmith et al. 2003; King et al. 1999) show that H_2O_2 concentrations will not reach these levels at the alpha dose rates prevailing within a failed container, and E_{CORR} values should always be within region A in Figure 9. Thus, as for O_2 , fuel corrosion in H_2O_2 solutions should generally be under cathodic control, but at a substantially greater rate than in O_2 solution. At such low potentials the anodic oxidation of

H_2O_2 ($\text{H}_2\text{O}_2 \rightarrow \text{O}_2 + 2\text{H}^+ + 2\text{e}^-$), which must couple to the cathodic reduction ($\text{H}_2\text{O}_2 + 2\text{e}^- \rightarrow 2\text{OH}^-$) to complete the decomposition process ($2\text{H}_2\text{O}_2 \rightarrow \text{O}_2 + 2\text{H}_2\text{O}$) is not observed, making peroxide decomposition within a failed container extremely unlikely. This makes fuel corrosion driven by H_2O_2 , as opposed to its decomposition product O_2 , the primary process.

As for O_2 reduction there is the possibility that H_2O_2 reduction could be catalyzed on an RE^{III} -doped surface and on epsilon particles. However, electrochemical studies detect no discernible influence of RE^{III} -doping and only a minor influence of epsilon particles, and then only at high degrees of simulated burnup (6 at%) (Goldik et al. 2006b). Thus, at the burnups achieved in CANDU fuel (~1.5 at%), no significant influence of epsilon particles on H_2O_2 reduction would be expected. This is a direct consequence of the ability of H_2O_2 to rapidly create $\text{U}^{\text{IV/V}}$ donor-acceptor sites making reduction on the fuel and on the epsilon particles only marginally different in rate, as opposed to the case with O_2 , when these rates are very different. This is illustrated in Figure 31. This means that the distinct separation of anodic and cathodic sites, which could lead to local acidification, Figure 21, is less likely with H_2O_2 than with O_2 .

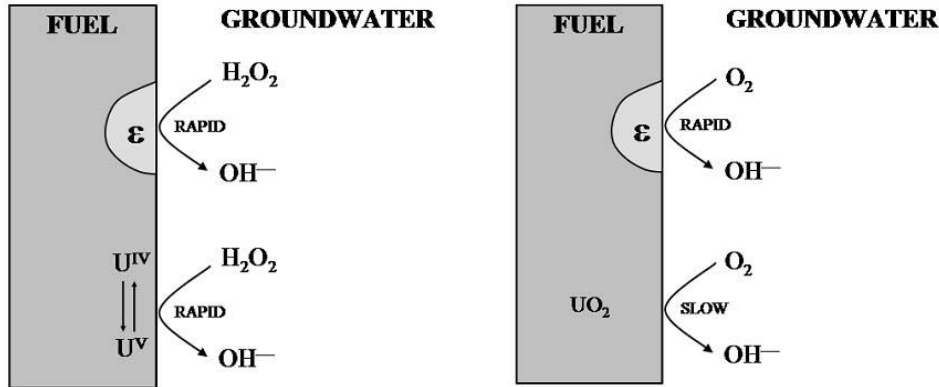


Figure 31: Illustrations showing that H_2O_2 reduction is rapid on both the fuel surface and epsilon particles, while the reduction of O_2 is only rapid on epsilon particles. The ability of H_2O_2 to oxidize the fuel surface and create $\text{U}^{\text{IV/V}}$ donor-acceptor sites makes H_2O_2 reduction kinetics rapid on both the fuel surface and epsilon particles. As a consequence, the kinetics on the two surfaces are hard to distinguish experimentally. By contrast, the inability of O_2 to similarly create $\text{U}^{\text{IV/V}}$ donor-acceptor sites means the kinetics of O_2 reduction on epsilon particles is much faster than on the UO_2 surface, making the two reactions are easily separated experimentally.

10. THE INFLUENCE OF REDOX SCAVENGERS PRODUCED BY CARBON STEEL CORROSION

As illustrated in Figure 11, fuel corrosion will occur inside a failed container also undergoing corrosion. Under the prevailing anoxic conditions, carbon steel will react with water to produce Fe^{2+} and H_2 ,



Thus, the situation inside the groundwater-flooded container comprises two corrosion fronts, interconnected by groundwater diffusion processes. The corrosion processes established on the two surfaces will occur at distinctly different E_{CORR} values, as illustrated in Figure 32. $(E_{\text{CORR}})_{\text{Fe}}$ will be ≤ -0.8 V under anoxic conditions (Blackwood et al. 1995; Smart et al. 2002a; Smart et al. 2002b; Lee et al. 2005) compared to $(E_{\text{CORR}})_{\text{UO}_2}$ values which are expected to be in the range -0.25V to -0.05V (line A in Figure 9). This large separation makes the corrosion products from each front thermodynamically unstable in the presence of those from the other, and introduces the possibility that the products of steel corrosion (Fe^{2+} , H_2) will scavenge the radiolytic oxidants (primarily H_2O_2) responsible for fuel corrosion. As depicted in Figure 11, redox scavenging will involve a series of homogenous reactions.

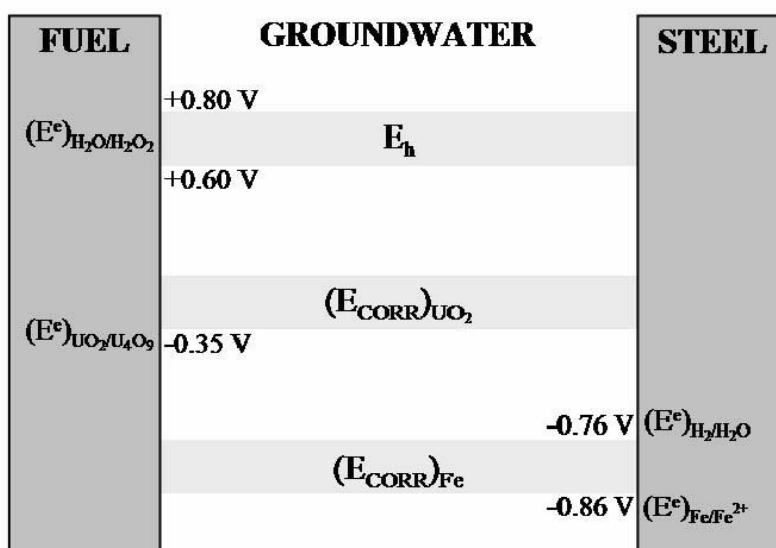


Figure 32: Illustration showing the two corrosion fronts existing within a failed, groundwater flooded waste container, one on the fuel surface established by reaction with radiolytic oxidants and a second one on the steel surface established by reaction with water. The zone marked E_h indicates the redox condition expected due to the alpha radiolysis of water. The E_{CORR} zones indicate the range of corrosion potentials measured on fuel and steel electrodes.

10.1 Scavenging by Ferrous (Fe^{II}) Ions

Ferrous ion (Fe^{II}) is a well known regulator of redox conditions in natural waters and its reaction with oxidants, in particular O_2 , has been extensively studied (Stumm 1990). The overall reaction can be written



where the exact speciation of Fe^{II} and Fe^{III} is determined by groundwater composition and pH. The reaction is highly pH dependent, with a rate that increases markedly with pH, and in neutral solution leads to the precipitation of Fe(OH)₃ (Tamura et al. 1976). The redox chemistry of the steel/iron oxide/soluble iron system, and its likely impact on fuel corrosion, has been reviewed in detail (Johnson et al. 2000; King et al. 2000).

Hydrogen peroxide will be consumed via the Fenton reaction (Jonsson et al. 2006; Sutton et al. 1989),



An effective G-value for H₂O₂ as low as 0.001 has been claimed for the Fe^{II}/Fe^{III} system (Christensen et al. 1982), and calculations based on alpha radiolysis models show that concentrations of Fe²⁺ in the expected groundwater range (~ 10⁻⁵ mol/L) can significantly arrest the rate of H₂O₂ production (Tait et al. 1986).

Studies on the influence of Fe and Fe corrosion products on fuel corrosion have been published (Shoesmith et al. 2003; Loida et al. 1996; Grambow et al. 1996; El Aamrani et al. 1998; Loida et al. 2006; Albinsson et al. 2003; Cui et al. 2003; Loida et al. 2001; Quinones et al. 2001; Ollila et al. 2003; Stroes-Gascoyne et al. 2002a, 2002b), and inevitably show that the presence of Fe suppresses the corrosion and the radionuclide release rates. Measurements over a period of 4.5 years demonstrated a reduction in Sr release rate by a factor of 460 due to the presence of Fe, where Sr release is taken as an indicator of the matrix corrosion rate. In tests with ²³³U-doped UO₂, U concentrations were lower than the solubility limit when active Fe was present (Ollila et al. 2003).

It is not possible to separate the scavenging effects of Fe²⁺ and H₂ in experiments with Fe since both are produced by steel corrosion. More direct attempts have been made to determine the influence of Fe²⁺ on fuel corrosion both experimentally (Quinones et al. 2001; Ollila et al. 2003) and via model calculations (Jonsson et al. 2006; King et al. 2002). Addition of Fe²⁺ to experiments with Pu-doped electrodes (Stroes-Gascoyne et al. 2002a, 2002b) showed that while Fe²⁺ concentrations of 10⁻⁵ mol/L did not influence E_{CORR}, a concentration of 10⁻⁴ mol/L suppressed it by 0.14 V, indicating a direct influence on the concentration of alpha radiolytically produced oxidants at the fuel surface. Calculations based on experimentally determined rate constants (Jonsson et al. 2006) indicated that the consumption of H₂O₂ via the Fenton reaction ([Fe^{II}] = 1 μmol/L) lead to substantial suppression of UO₂ dissolution (> a factor of 40). By contrast, calculations using a mixed potential model (King et al. 2002) indicated only a minor effect of Fe²⁺. The difference between these two calculations is the presence of a corrosion product deposit in the latter, but not the former, calculation. This deposit acts as a diffusion barrier limiting access of dissolved Fe²⁺ to the fuel surface where the peroxide is radiolytically produced.

10.2 Scavenging by Hydrogen

Measured corrosion rates for steel under simulated granitic groundwater conditions are in the range 0.05 to 0.1 μm/year (Smart et al. 2002a; Smart et al. 2002b). In sealed repositories, this would lead to the establishment of H₂ pressures greater than 5 MPa (Carbol et al. 2005), and

dissolved groundwater concentrations in the 10 to 100 mmol/L range, leading to the possibility that H₂ could be a scavenger for radiolytic H₂O₂.

The suppression of fuel corrosion and radionuclide release in the presence of H₂ is consistently observed, well documented (Grambow et al. 2000; Spahiu et al. 2000; Spahiu et al. 2004; Rollin et al. 2001), and recently reviewed (Carbol et al. 2005; Poinssot et al. 2005). The effect is very large, a decrease in corrosion rate of over four orders of magnitude (compared to rates under oxidizing conditions) being observed in H₂-purged experiments ([H₂] ~ 0.8 mmol/L) (Rollin et al. 2001). These experiments were conducted using a flow through technique, and the influence of solution flow rate indicates that slow hydrogen replenishment allows an increase in the radiolytic corrosion rate. For high burnup fuels (~50 MWd/kgU) with substantially higher radiation dose rates leached in 5.0 mol/L NaCl for over 1000 days (Carbol et al. 2005; Poinssot et al. 2005), an H₂ pressure of 0.32 MPa suppressed the U concentrations to ~10⁻⁹ mol/L, which approaches the measured solubility (10^{-9.5} mol/L) for UO₂ (section 3). The concentration of other redox sensitive radionuclides, whose release rate would be expected to depend on radiolytic corrosion, were also extremely low. The observation that radiolytic oxygen levels were below the detection limit (10⁻⁸ mol/L) over the full duration of the experiment clearly suggested that consumption of radiolytic oxidants by H₂ could account for the low corrosion rates.

Experiments (with an H₂ pressure of 5.3 MPa; [H₂] ~ 43 mmol/L) with much higher alpha-active MOX fuel confirmed these observations, concentrations of U falling over 494 days to 3 x 10⁻¹⁰ mol/L which is effectively the reported solubility for UO₂. The measurement of initially high U concentrations in these experiments is common, and can be attributed to the relatively rapid dissolution of a preoxidized surface layer present on the fuel due to air exposure. In this experiment, no corrosion rate could be calculated, since the U concentration did not increase over the 494 days. These studies show that the release rate of the majority of radionuclides decreases almost linearly with increasing H₂ pressure with fractional inventory release rates of only 10⁻⁹ /day achieved at a H₂ partial pressure as low as 0.01 to 0.1 MPa ([H₂] of 0.027 to 0.27 mmol/L in 5.0 mol/L NaCl).

Similar results were obtained with an alpha-doped UO₂ containing 10 wt% ²³³U, manufactured to simulate spent fuel a few thousand years after discharge from the reactor. As with spent fuel, U concentrations were effectively equal to the solubility of UO₂ (3 x 10⁻¹⁰ mol/L), and radiolytic oxygen undetectable, throughout the experiment. These conditions were maintained despite periodic reductions in H₂ pressure from 1.6 MPa ([H₂] ~ 10 mmol/L) to 0.016 MPa ([H₂] ~ 0.01 mmol/L), and subsequent XPS analysis found no detectable oxidation of the UO₂ surface. It would appear that a concentration of dissolved H₂ as low as 10⁻² mmol/L is sufficient to prevent radiolytic corrosion of UO₂ with an average α-dose rate in a 35 μm layer of water at the surface of the fuel of 99 Gy/hour. Inspection of Figure 7 shows this is effectively the maximum average alpha dose rate expected in CANDU fuel (of average burnup).

These results cannot be explained by the scavenging of radiolytic oxidants involving reaction with H₂ in the bulk of solution. Alpha radiolysis of aqueous solutions shows that dissolved H₂ concentrations in the range 0.008 to 0.8 mmol/L (0.001 to 0.01 MPa H₂) had no influence on the production of radiolytic oxidants (Pastina et al. 2001), and Nilsson et al. (2007) found that the rate of reaction of H₂O₂ with UO₂ was uninfluenced by the presence of H₂. These observations suggest that the consumption of radiolytic oxidants by H₂ is a surface catalyzed process.

Ample experimental evidence exists to support this claim, with H₂ having been shown to reduce the extent of fuel oxidation in the presence of both gamma (King et al. 1999; King et al. 2004) and alpha (Sunder et al. 1990) radiation. An influence in the presence of gamma radiation is not surprising, since standard radiolysis models show that H₂O₂ production is suppressed by reaction with low concentrations (10⁻² mol/L) of H₂ to produce H• and OH• radicals which recombine to H₂O (Tait et al. 1986). However, irradiation of UO₂ in the presence of H₂ (5 MPa; [H₂] ~ 4 mmol/L) suppressed E_{CORR} to values in the range -0.5 V to -0.82 V compared to values measured in the presence of gamma radiation only or in unirradiated Ar-purged solutions, Figure 33 (King et al. 2004). The magnitude of this effect is illustrated in Figure 34, which compares these values to the range of E_{CORR} values measured under different oxidizing conditions (King et al. 2004). A most likely explanation for this effect is that H• radicals react with OH• (produced from H₂O₂ involved in fuel oxidation) to yields water, thereby scavenging the oxidant which drives fuel corrosion. Additional unidentified features of the effect of H₂ on fuel exist, and it has been speculated that the slow decrease in E_{CORR} indicates reduction of U^V species in the oxide. These effects appear partially irreversible since H₂ “reduced” surfaces reoxidize to a lesser degree than surfaces not previously exposed to H₂ (King et al. 2004).

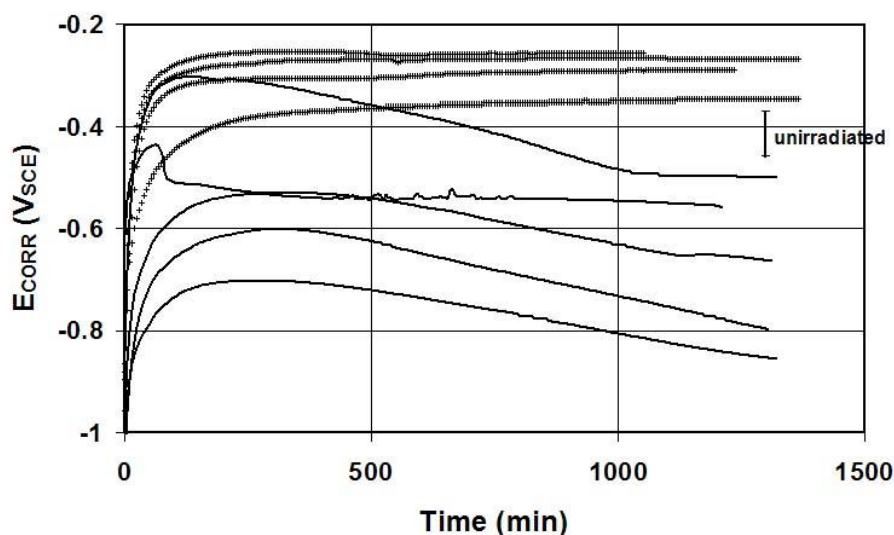


Figure 33: Time dependence of the corrosion potential (E_{CORR}) of a UO₂ electrode in gamma-irradiated 0.1 mol/L NaCl (pH~9.5) at room temperature in the presence of either 5MPa of H₂ or Ar. The results of four or five replicate tests are shown for each set of conditions. The range of E_{CORR} values recorded in unirradiated solutions for both gases is shown as the vertical bar (King and Shoemsmith 2004).

XPS analyses showed that the extent of oxidation of UO₂ specimens exposed to external alpha radiation sources increased with increasing alpha source strength when H₂ was not present but not when it was (~0.16mmol/L) (Sunder et al. 1990). While these studies support claims that a combination of alpha radiolysis and H₂ suppresses fuel corrosion, the high temperature employed (100°C) leaves unanswered the question of whether H₂ was activated (i.e. decomposed to reactive H• radicals) thermally or radiolytically.

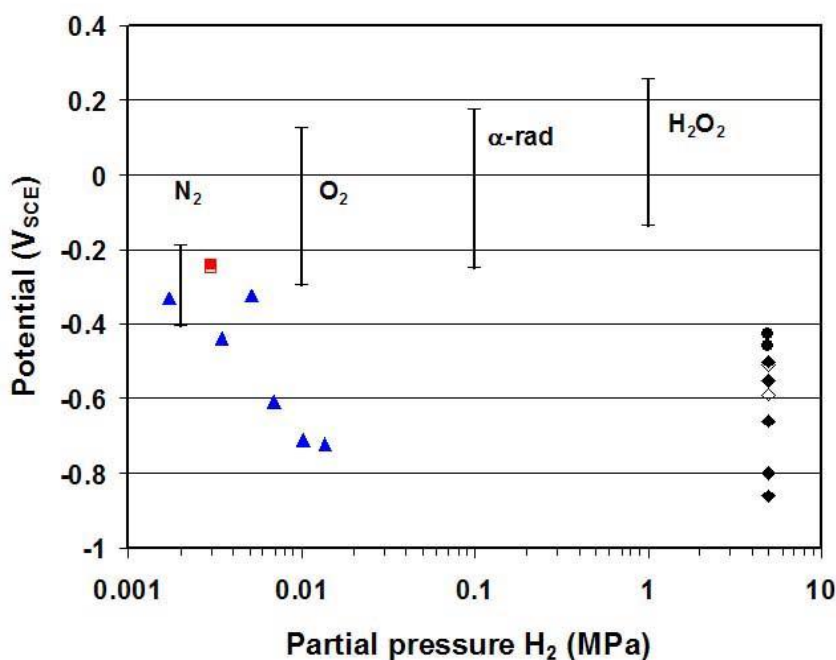


Figure 34: Corrosion potential (E_{CORR}) values measured on UO_2 at 5 MPa of H_2 , and on 1.5 at% SIMFUEL at various H_2 pressures, compared to the ranges of values measured under various anoxic and oxidizing conditions (King and Shoemsmith 2004). The SIMFUEL values (\blacktriangle) are taken from Figure 35 just before changes in gas pressure. The ranges of E_{CORR} values are for deaerated solutions (N_2), O_2 -purged solutions (10^{-8} to 1.4×10^{-3} mol/L), alpha radiolysis (α -rad) (alpha source strengths from 4 to 800 μCi), and H_2O_2 solutions (10^{-6} to 10^{-1} mol/L) (King and Kolar 2002), and are shown at arbitrary H_2 pressures for clarity.

Exactly how alpha radiation activates H_2 is not known, but has been discussed (Carbol et al. 2005). The radiation-induced generation of H_2 from water adsorbed on oxides surfaces has been investigated on a number of oxides (Petrick et al. 2001), and shown to occur on UO_2 (Laverne et al. 2003). Heavy ion sputtering of the UO_2 surface to produce oxygen vacancies (a process similar to the alpha recoil process on emission of an α -particle) enhanced the formation of atomic hydrogen (H^\bullet) (Stultz et al. 2004). The reduction of H_2O_2 to repair this surface damage could also proceed through an OH^\bullet radical intermediate, and its reaction with H_2 could produce an additional H^\bullet ($\text{OH}^\bullet + \text{H}_2 \rightarrow \text{H}_2\text{O} + \text{H}^\bullet$), leading to the suppression of oxidation and corrosion.

For spent fuels, H_2 activation on noble metal (epsilon) particles is likely to prove a more important mechanism for suppressing fuel corrosion than the utilization of defects produced by alpha recoil (Cui et al. 2004; Nilsson et al. 2007). This process has been electrochemically characterized in detail using SIMFUEL specimens with different levels of simulated burnup (Broczkowski et al. 2005; Broczkowski et al. 2007; Broczkowski et al. 2006). The E_{CORR} on SIMFUEL is significantly decreased in solutions purged with only small amounts of H_2 and, even for a low density of epsilon particles, can be reduced to values well below the -0.4 V threshold for the onset of fuel corrosion, Figure 35 (Broczkowski et al. 2005). The value of E_{CORR}

achieved decreases with the number density of epsilon particles present, Figure 36, and analyses confirm that the extent of oxidation of the surface decreased as E_{CORR} was suppressed, Figure 36. As illustrated schematically in Figure 37, this effect can be attributed to the reversible dissociation of H_2 (to H^\bullet radicals) on the epsilon particles that act as galvanically-coupled anodes within the fuel matrix, thereby decreasing E_{CORR} and inhibiting UO_2 oxidation/corrosion. As indicated by the arrow in Figure 9, only chemical dissolution can occur under these conditions.

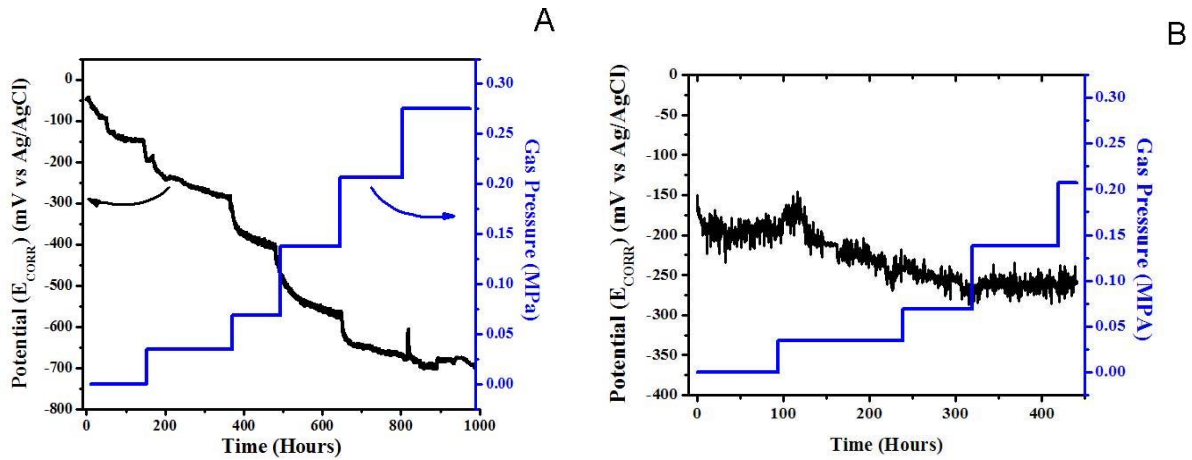


Figure 35: The influence of H_2 solution overpressure on the corrosion potential of a 1.5 at% SIMFUEL containing epsilon particles (A) and a 1.5 at% SIMFUEL with no epsilon particles (B). E_{CORR} measurements were made at $60^\circ C$ in a pressure vessel in a 0.1 mol/L KCl solution ($pH = 9.5$). The system was initially purged with Ar only at atmospheric pressure, and then with a series of increasing 5% H_2/Ar pressures (Broczkowski et al. 2005).

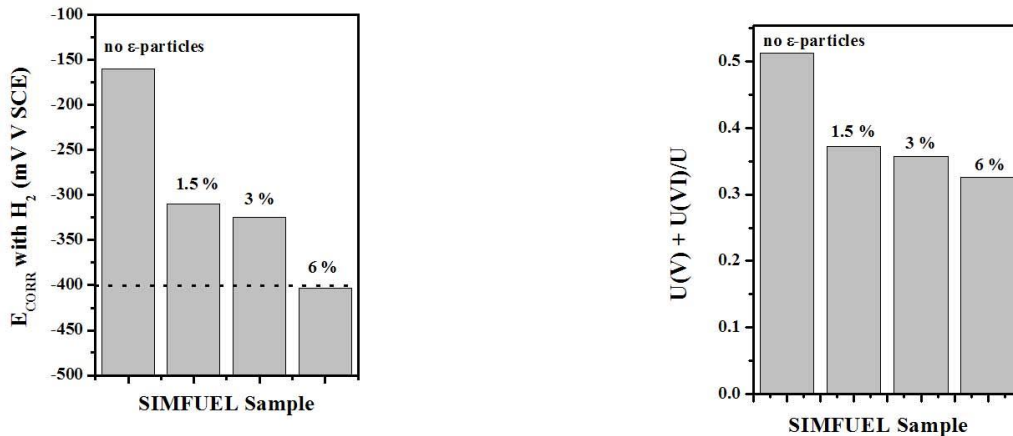


Figure 36: The influence of the increasing number and size of epsilon particles in SIMFUELS with different degrees of simulated burnup on the corrosion potential (E_{CORR}) and the degree of oxidation of the surface in H_2 -purged 0.1mol/L KCl. The horizontal line indicates the potential threshold below which the corrosion of the UO_2 surface will not occur (from Figure 9).

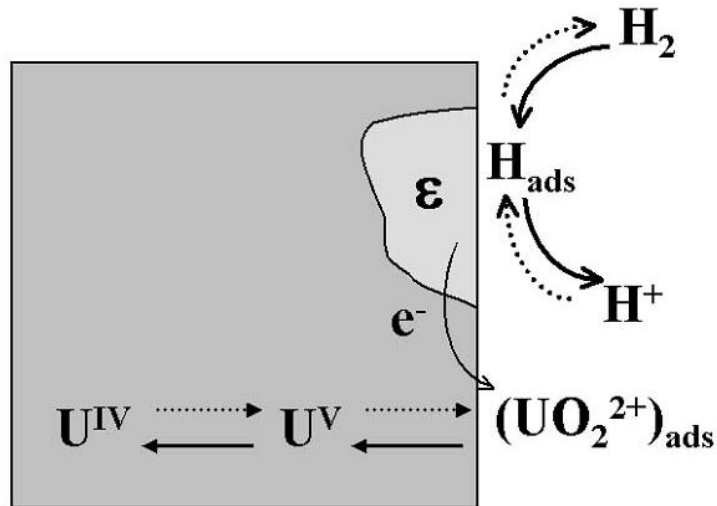


Figure 37: Illustration showing the galvanic coupling of epsilon particles to the fuel matrix in H₂-containing solutions. In the presence of dissolved H₂ in the solution, the rapid kinetics of the H₂ oxidation/H⁺ reduction reaction on the particles suppresses the potential of the particle. Since the particles are galvanically coupled to the matrix, the potential of UO₂ is drawn to the same value, and for a sufficient H₂ concentration, the potential is suppressed to a value more negative than the threshold value for fuel corrosion (0.4 V in Figure 9). When this occurs, the fuel is galvanically protected from corrosion (Broczkowski et al. 2005).

11. FUEL CORROSION/DISSOLUTION RATES

A comprehensive review of rates for UO₂ and used fuels has been published (Oversby 1999). Rates measured for spent fuels in aerated neutral solutions are generally in the range 1 to 7 mg/m²/d (Rollin et al. 2001; Gray et al. 1995; Gray 1998; Grambow et al. 1994; Werme et al. 1989; Forsyth 1997) with the higher rates more likely in carbonate-containing solutions. Similar values, in the range 2 – 4 mg/m²/d when carbonate is present, were observed for UO₂ (Shoesmith et al. 1996). This similarity suggests the properties of the spent fuel surface are of secondary importance in determining the corrosion rate. Under static leaching conditions in the absence of carbonate, when the formation of corrosion product deposits would be expected, rates for UO₂ in the range 0.0003 to 0.006 mg/m²/d are observed in neutral (pH = 8) solution compared to 0.08 to 0.2 mg/m²/d in flow through experiments when deposits should be avoided (Casas et al. 1991). This comparison suggests that the influence of deposits in suppressing the corrosion rate could be as small as a factor of 13 or as large as a factor of 660. According to Oversby, this wide range reflects the uncertainties in the measurements and cannot, therefore, be taken as a quantitative indication of the influence of corrosion products.

Despite the scatter in the values, Figure 38 (from Poinssot et al. 2005) shows a clear dependence of corrosion rate on the specific alpha activity (as illustrated schematically in Figure 10), and a threshold below which the rate becomes independent of activity. The data in this plot is from a large number of individual experiments. This threshold appears to be located between 3.5 and 33 MBq/g_{UO₂}, as indicated by the vertical lines in the figure. If the dose rates to

solution for the upper and lower limits of this threshold are compared to the dose rates calculated for a CANDU fuel bundle with a burnup of 220 MWh/kgU, as indicated by the horizontal lines in Figure 39, it can be seen that the alpha dose rate of the fuel only marginally exceeds the upper limit and only at short times (≤ 300 -400 years). Two observations can be made; (i) the corrosion rate measured for the upper limit of this threshold can be considered the maximum sustainable by alpha radiolysis for CANDU fuel; and (ii), no radiolytic corrosion should be observed for CANDU fuel beyond $\sim 10,000$ to 20,000 years, when the alpha dose rate falls below the lower threshold limit.

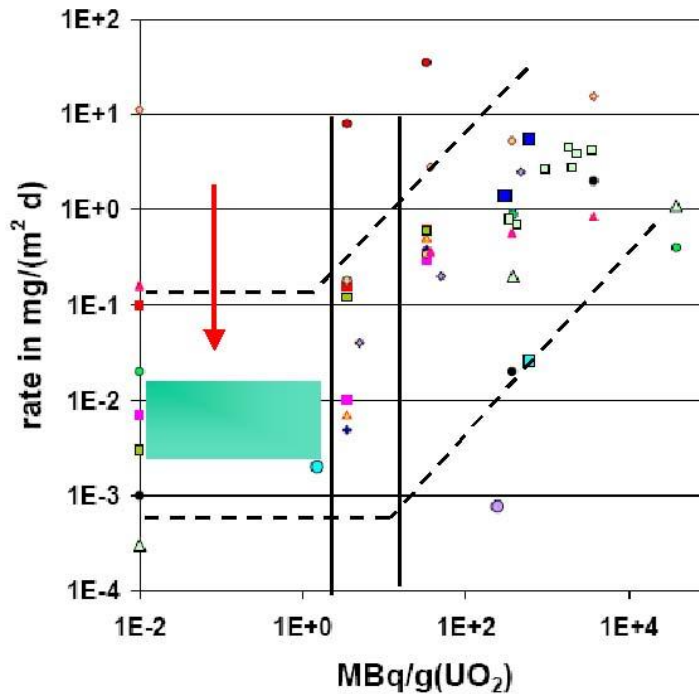


Figure 38: Corrosion rates measured as a function of specific alpha activity on alpha-doped electrodes, undoped UO_2 (10^{-2} M Bq/g) and spent fuel (Figure 25 in Poinssot et al. 2005). The vertical black lines indicate the approximate location of the specific alpha activity threshold, below which no effect of alpha activity on the corrosion rate is observed. As indicated in the schematic illustration in Figure 10, this threshold represents the alpha activity level at which the fuel dissolution process switches from radiolytic control to solubility control. The dashed lines are arbitrary and drawn to illustrate the dependence and independence of the rate on alpha activity above and below the threshold, respectively. The shaded zone shows the values of corrosion rate predicted around the corrosion threshold established electrochemically (Figures 8 and 9) using a simple model to extrapolate rates measured electrochemically [Shoosmith and Sunder 1991]. The vertical arrow shows the corrosion rates predicted using a mixed potential model developed to determine the influence of alpha radiolysis on CANDU fuel corrosion (Shoosmith et al. 2003). The upper value is the rate predicted on first failure of the waste container. The lower rate is the value predicted to prevail after 10^6 years.

To determine whether the rates measured in the region of this proposed threshold for alpha activity are consistent with those predicted for the electrochemically established threshold for radiolytic corrosion around an E_{CORR} of -0.4 V (Figure 9), a simple electrochemical model can be used to predict the corrosion rate at this threshold potential (Shoesmith et al. 1991). The model involves the extrapolation of electrochemically measured anodic dissolution currents as a function of potential and has been used previously to predict the influence of radiolytic oxidants on fuel corrosion (Sunder et al. 1997). The same relationship between current and potential is used in the more complex and mechanistically detailed mixed potential model (Shoesmith et al. 2003).

The shaded area in Figure 38 shows the rates predicted for the E_{CORR} range, -0.35 V to -0.45 V (chosen to bracket the threshold value of -0.4 V), and confirms that the electrochemically-predicted threshold is consistent with direct dissolution rate measurements. Also shown in Figure 38 (by the vertical arrow) is the decrease in corrosion rate predicted over a 10^6 year period by the MPM, a model which accounts only for the influence of alpha radiolysis (Shoesmith et al. 2003). The maximum rate predicted by this model should be consistent with the measured value of the rate at the upper limit of the threshold, since this is approximately the maximum dose rate that should prevail at short times, Figure 38, when failure is assumed to occur in the model. Inspection of Figure 39 shows this is the case. However, the rate is not predicted to approach the threshold value even after 10^6 years (the bottom end of the arrow in Figure 39), despite the indication based on expected dose rates that this threshold should have been reached after $\sim 10,000$ to $20,000$ years, Figure 39. Since neither the measurements of corrosion rates with alpha-doped specimens nor the simple electrochemical extrapolation take account of the formation of corrosion product deposits whereas the MPM does, this discrepancy can be attributed to the confinement of radiolytic oxidants (primarily H_2O_2) within pores in such a deposit. A clearer understanding of the influence of deposits is required to clarify the significance of this discrepancy.

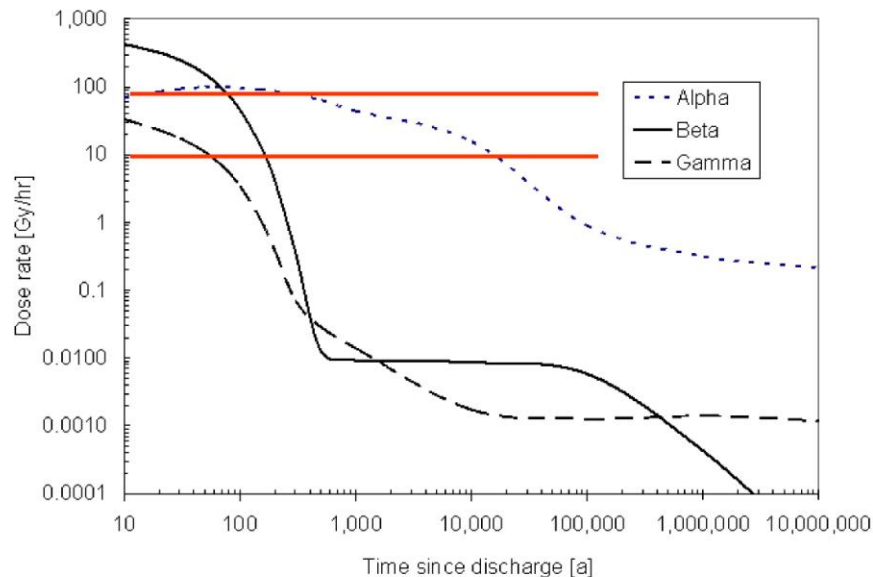


Figure 39: Alpha, beta and gamma radiation dose rates calculated as a function of time for a layer of water in contact with a CANDU fuel bundle with a burnup of 220 MWh/kgU. The two horizontal lines represent the upper and lower limits of the alpha activity threshold as defined by the two vertical lines in Figure 38.

A comparison of electrochemically-predicted corrosion rates to spent fuel rates measured with and without H₂ can also be made. Figure 40 shows fuel corrosion/dissolution rates based on U analyses, and the congruent release of ¹³⁷Cs, for aerated and H₂-purged conditions (Rollin et al. 2001). As noted in section 10.2, the corrosion rate under H₂-purged conditions ([H₂] ~ 8 mmol/L) is orders of magnitude lower than observed for aerated conditions. The corrosion rates obtained under aerated conditions are consistent with the measurements reviewed by Oversby (Oversby 1999). The two horizontal lines bracket the corrosion rates derived by extrapolating experimental (electrochemical current) data to the potential threshold of -0.4 V (-0.35 V to -0.450 V) determined electrochemically. The coincidence between electrochemically-predicted and experimentally measured rates confirm that even a small concentration of H₂ is sufficient to suppress corrosion rates to the radiolytic threshold, even when substantial γ/β radiation fields are present.

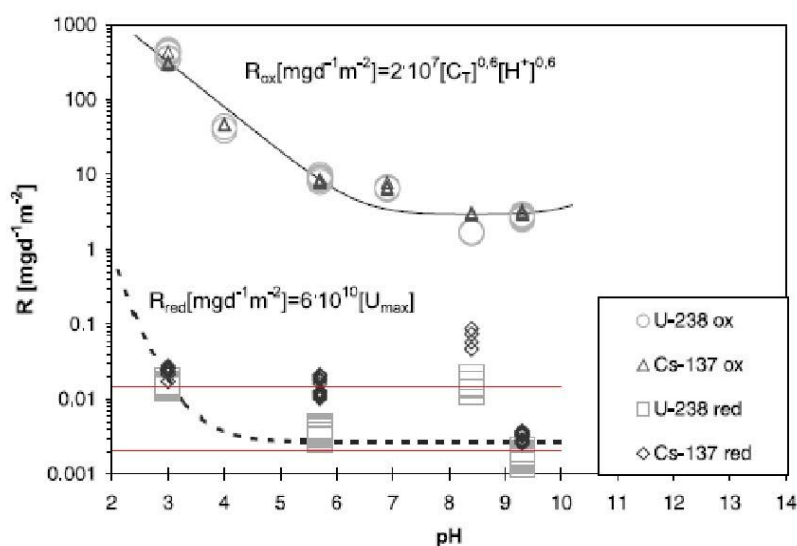


Figure 40: Used fuel dissolution rates, based on dissolved ²³⁸U and ¹³⁷Cs concentrations as a function of pH for oxidizing and reducing conditions. Measurements were performed in a single-pass flow-through apparatus [Rollin et al. 2001]. Experiments under oxidizing conditions were conducted in a solution purged with a gas mixture containing 20% O₂/0.03% CO₂/80% Ar. Reducing conditions were achieved by bubbling H₂ containing 0.03% CO₂ over a Pt foil. The two horizontal lines bracket the corrosion rates derived by extrapolating experimental data to the potential threshold of -0.4 V (-0.35 V to -0.45 V) determined electrochemically (Figures 8 and 9)

Corrosion rates remain measurable in these spent fuel experiments. It is possible that some influence of radiolysis still persists, since rates increased slightly with decreasing solution flow rates, indicating H₂ depletion to a level at which it could not totally neutralize radiolytic oxidants. However, that H₂ can completely suppress radiolytic corrosion has been demonstrated using a 10 wt% ²³³U-doped specimen when no U dissolution was measurable over a period of greater than 800 days. Based on this experiment it was calculated that a dissolved H₂ concentration of 10⁻² mmol/L was sufficient to completely suppress the alpha-radiolytic corrosion of UO₂ with an average dose rate (over a 35 μm layer of water) of 99 Gy/hour. Since average alpha dose rates

in CANDU fuel are never expected to exceed this level and H₂ concentrations are expected to rise to 10 to 100 mmol/L under repository conditions, an argument can be made that radiolytic corrosion of CANDU spent fuel will, at the worst, be a short term occurrence.

12. CONCLUSIONS

The primary factor controlling the rate of corrosion of CANDU fuel inside a failed waste container will be the redox condition at the fuel surface, how it evolves with time, and how it is influenced by the presence of scavengers, especially H₂, produced by the corrosion of the steel liner in the container. If the container fails while gamma/beta radiation fields are significant (\leq 1000 years), oxidizing conditions would be established. If these radiation fields have decayed to insignificant levels before failure occurs, then the redox conditions established by alpha radiolysis will be only mildly oxidizing.

Redox conditions will become less oxidizing with time as radiation fields decay. Electrochemical studies have identified a specific potential below which the UO₂ will be immune to corrosion. This potential threshold is well established based on surface analysis methods and has been shown to predict, with reasonable accuracy, a specific alpha activity threshold based on corrosion rate measurements on alpha-doped UO₂ specimens. For CANDU fuel in the expected burnup range of 120 to 320 MWh/kgU, this threshold appears to be reached after 10,000 to 20,000 years, although some uncertainty still exists. Below this threshold only chemical dissolution of the fuel (UO₂ → U(OH)₄), as opposed to radiolytically driven corrosion (UO₂ → UO₂²⁺) is possible.

If conditions are oxidizing many issues arise.

- (a) The primary radiolytic oxidant will be H₂O₂. Any influence of O₂, which can form radiolytically and by the decomposition of H₂O₂, will be marginal. This is because the kinetics of its reaction with UO₂ is over two orders of magnitude slower than those of H₂O₂, and its formation by H₂O₂ decomposition is not expected under anticipated conditions within a failed container.
- (b) The formation of corrosion product deposits will occur on the corroding fuel surface. Deposition would be enhanced if calcium and silicate concentrations in the groundwater are high, since these species will decrease the solubility of dissolved U (as UO₂²⁺) leading to the formation of calcium-containing hydrated U^{VI} silicate phases. The formation of these deposits would suppress the corrosion rate by reducing the area of the fuel surface exposed to corrosion in the groundwater.
- (c) If sufficiently rapid, anodic oxidation of the fuel, followed by hydrolysis of dissolved UO₂²⁺, could produce local acidic conditions within pores in the deposit or within flaws, such as the site of missing grains, in the fuel surface. This acidification can only occur if the anodic fuel dissolution site is separated from the cathodic oxidant reduction site, to avoid its neutralization, at least partially, by the alkalinity produced by H₂O₂ reduction. Although unlikely, the separation of anodes and cathodes involved in fuel corrosion is possible, since the noble metal (epsilon) particles could act as preferential cathodes.
- (d) In groundwaters containing bicarbonate, the extent of corrosion product deposition would be decreased, since HCO₃⁻ can complex UO₂²⁺ and significantly increase its solubility. The HCO₃⁻/CO₃²⁻ equilibrium would also buffer the pH and suppress the formation of local acidity within the deposit or fuel surface flaws. The suppression of deposition would increase the area of UO₂ exposed to corrosion in groundwater. This,

coupled with the complexing ability of the HCO_3^- would lead to an increase in corrosion rate. For the conditions anticipated in the Canadian Shield groundwaters, carbonate concentrations are likely to be $< 10^{-3}$ mol/L, and the primary influence of HCO_3^- would be on the extent of deposition, with only a small direct effect on the kinetics of the corrosion process.

- (e) In-reactor burnup, which is low in CANDU used fuel compared to fuel from other reactors, will have only a minor to insignificant effect on fuel corrosion, despite the increased fuel conductivity due to fission product doping of the UO_2 lattice and the presence of epsilon particles. No influence of doping at CANDU burnup levels was observed on the anodic dissolution of UO_2 , and the cathodic reduction of H_2O_2 on the epsilon particles was only marginally faster than on the surface of the UO_2 matrix.

For the mildly oxidizing conditions expected when only the alpha radiolysis of water is possible, most of these issues become much less important.

- (a) While corrosion deposits may still form and partially block corrosion, the rate of fuel dissolution within pores and surface flaws should not produce locally acidic conditions, even if anodic and cathodic sites are separated.
- (b) The ability of HCO_3^- to accelerate fuel corrosion begins to disappear as control of the overall process switches from the anodic dissolution reaction, which can be accelerated by HCO_3^- , to the cathodic reaction, which cannot. The cathodic reaction would be kinetically-limited by the small concentration of available oxidants at the relatively low alpha radiation dose rates.

When alpha radiation fields decay below the levels expected between 10,000 and 20,000 years, redox conditions reach the threshold level at, or below, which radiolytic corrosion of the fuel will not occur. For times greater than this, the overall process becomes chemical dissolution, and would be controlled by the solubility of the U^{IV} state, which a number of independent measurements show to be extremely low.

Under these conditions, the used fuel dissolution rate will be controlled by its solubility, the diffusion coefficient of dissolved species in the groundwater, and the groundwater flow rate. Within a failed container, groundwater would be expected to be stagnant, making the overall dissolution/radionuclide release rate diffusion-controlled.

Under these anoxic conditions, the U solubility and, hence, the fuel dissolution rate will be relatively insensitive to groundwater composition, since the U^{IV} state is readily hydrolyzed. This will make the solubility slightly pH-dependent, but insensitive to complexation by the anions present in the groundwater. In calcium and silicate-containing groundwaters, alteration to less soluble U^{IV} solids containing these species is thermodynamically possible, and could lead to the acceleration of radionuclide release. However, the kinetics of these alteration processes appear to be extremely slow, since such phases have not been observed in laboratory experiments and occur to only a marginal extent in natural deposits, such as the Cigar Lake uranium ore deposit.

The transition from radiolytic corrosion to chemical dissolution can be very rapidly induced in the presence of redox scavengers, especially H_2 , produced by the corrosion of the steel liner in the container. Small concentrations of H_2 can suppress the redox condition to the threshold for radiolytic corrosion, even for used fuels with high gamma/beta radiation fields. The absence of radiolytic oxidants in experiments with used fuel indicates that they are very efficiently scavenged by the presence of hydrogen.

If only alpha radiation is present (in alpha-doped UO_2), the presence of small concentrations of H_2 reduces the U dissolution rate to immeasurable values over periods of 2 to 3 years. On specimens containing epsilon particles, which are known to be catalytic for the H_2/H^+ reversible reaction, small hydrogen concentrations can suppress the redox condition of the fuel surface (the corrosion potential) to well below the threshold, effectively leading to galvanic protection of the fuel matrix against corrosion.

While the mechanistic details of the reaction of H_2 with potential oxidants on the fuel surface remain to be resolved, it is clear that the fuel surface is involved. This has been clearly demonstrated for fuel containing epsilon particles and fuels containing alpha dopants.

Since the production of H_2 will commence as soon as the steel surfaces within the container are wetted with groundwater, this influence of H_2 has the potential to shut down fuel corrosion very rapidly even while redox conditions are potentially oxidizing; i.e., even if container failure occurs while gamma/beta radiation fields are still significant. It is possible, therefore, that the transition from radiolytic corrosion to chemical dissolution of the fuel will occur very rapidly and fuel dissolution, and, hence, radionuclide release will be extremely slow almost from the time of container failure. Additional research to verify this claim is required.

ACKNOWLEDGEMENTS

This research was funded under the Industrial Research Chair agreement between NSERC, Ontario Power Generation, and The University of Western Ontario. The contributions of the many research groups at The University of Western Ontario, who have contributed to the development of understanding of fuel behaviour, are gratefully acknowledged. These members include, Billy Santos, Jon Goldik, Charmaine Lee, Michael Broczkowski, Heming He, Derrick Ofori, Peter Keech, Woo-Jae Cheong, Zack Qin, and Jamie Noel.

REFERENCES

- Albinsson, Y., A. Odegaard- Jensen, V.M. Oversby and L.O.Werme. 2003. Leaching of spent fuel under anaerobic and reducing conditions, *Mat. Res. Soc. Symp. Proc.* 757, 407-413.
- Amme, M. 2002. Contrary effects of the water radiolysis product H_2O_2 upon the dissolution of nuclear fuel in natural ground water and deionized water, *Radiochim. Acta* 90, 399-406.
- Amme, M., B. Renker, B. Schmid, M.P. Feth, H. Bertagnolli and W. Dobelin. 2002. Raman microspectrometric identification of corrosion products formed on UO_2 nuclear fuel during leaching experiments, *J. Nucl. Mater.* 306, 202-212.
- Amme, M., T. Wiss, H. Thiele, P. Boulet and H. Lang. 2005. Uranium secondary phase formation during anoxic hydrothermal leaching processes of UO_2 nuclear fuel, *J. Nucl. Mater.* 341, 209-223.
- Anastasijevic, N.A., Z.M. Dimitrijevu and R.R. Adzic. 1986. Oxygen reduction on a ruthenium electrode in alkaline electrolytes, *J. Electroanal. Chem.* 199, 351-364.

- Bailey, M.G., L.H. Johnson and D.W. Shoesmith. 1985. Effects of alpha radiolysis of water on the corrosion of UO_2 , *Corros. Sci.* 25, 233-238.
- Betteridge, J.S., N.A.M. Scott, D.W. Shoesmith, L.E. Bahen, W.H. Hocking and P.G. Lucuta. 1997. Effects of hyperstoichiometry and fission products on the electrochemical reactivity of UO_2 nuclear fuel, Atomic Energy of Canada Ltd. Report, AECL-11647, COG-96-331-1.
- Blackwood, D.J., C.C. Naish, N. Platts, K.J. Taylor and M.I. Thomas. 1995. The anaerobic corrosion of carbon steel in granite groundwater, Swedish Nuclear Fuel and Waste Management Company, Technical Report, TR-95-03.
- Broczkowski, M.E., J.J. Noel and D.W. Shoesmith. 2005. The inhibiting effects of hydrogen on the corrosion of uranium dioxide under nuclear waste disposal conditions, *J. Nucl. Mater.* 346, 16-23.
- Broczkowski, M.E., J.J. Noel and D.W. Shoesmith. 2007. The influence of temperature on the anodic oxidation/dissolution of uranium dioxide, *Electrochim. Acta*, accepted for publication.
- Broczkowski, M.E., J.J. Noel and D.W. Shoesmith. 2007. The influence of dissolved hydrogen on the surface composition of doped uranium dioxide under aqueous corrosion conditions, *J. Electroanal. Chem.* 602, 8-16.
- Broczkowski, M.E., R. Zhu, Z. Ding, J.J. Noel and D.W. Shoesmith. 2006. Electrochemical, SECM and XPS studies of the influence of H_2 on UO_2 nuclear fuel corrosion, *Mat. Res. Soc. Symp. Proc.* 932, 449-456.
- Brown, R.A. 1980. Uranium precipitation with hydrogen peroxide, *Soc. Min. Eng. AIME* 270, 1836-1840.
- Buck, E.C., D.J. Wronkiewicz, P.A. Finn and J.K. Bates. 1997. A new uranyl oxide hydrate phase derived from spent fuel oxidation, *J. Nucl. Mater.* 249, 70-76.
- Buck, E.C., R.J. Finch, P.A. Finn and J.K. Bates. 1998. Retention of neptunium alteration phases formed during spent fuel corrosion. *Mat. Res. Soc. Symp. Proc.* 506, 83-89.
- Burns, P.C., K. M. Deely and S. Skanthakumar. 2004. Neptunium incorporation into uranyl compounds that formed as alteration products of spent nuclear fuel. Implications for geologic repository performance, *Radiochim. Acta* 92, 151-160.
- Burns, P.C., R.C. Ewing and M.L. Miller. 1997. Incorporation mechanisms of actinide elements into the structure of U^{6+} phases formed during the oxidation of spent nuclear fuel, *J. Nucl. Mater.* 245, 1-9.
- Burns, P.C., R.J. Finch, F.C. Hawthorne, M.L. Miller and R.C. Ewing. 1997. The crystal structure of lanthanite, $[\text{U}_2^{4+}(\text{UO}_2)_4\text{O}_6(\text{OH})_4(\text{H}_2\text{O})_4](\text{H}_2\text{O})_5$: a possible phase for Pu^{4+} incorporation during the oxidation of spent nuclear fuel, *J. Nucl. Mater.* 249, 199-206.

- Carbol, P., J. Cobos-Sabate, J-P. Glatz, C. Ronchi, V. Rondinella, D.H. Wegen, T. Wiss, A. Loida, V. Metz, B. Kienzler, K. Spahiu, B. Grambow, J. Quinones, A. Martinez Esparza Valiente. 2005. The effect of dissolved hydrogen on the dissolution of ^{233}U -doped UO_2 (s), high burn-up spent fuel and MOX fuel, Swedish Nuclear Fuel and Waste Management Company, Technical Report TR-05-09.
- Casas, I., J. Gimenez, V. Marti, M.E. Torrero and J. de Pablo. 1991. Kinetic studies of unirradiated UO_2 dissolution under oxidizing conditions in batch and flow-through experiments, *Radiochim. Acta* 66/67, 23-27.
- Cheong, W.J., P.G. Keech, J.C. Wren. Z. Qin and D.W. Shoesmith. 2007. Modelling the distribution of acidity within nuclear fuel (UO_2) corrosion product deposits and porous sites; to appear in *Mat. Res. Soc. Symp. Proc.* 2007.
- Choi, J.W., R.J. McEachern, P. Taylor, and D.D. Wood. 1996. The effect of fission products on the rate of U_3O_8 formation in SIMFUEL oxidized in Air at 250°C , *J. Nucl. Mater.* 230, 250-258.
- Christensen, H., and E. Bjergbakke. 1982. Radiolysis of groundwater from spent fuel, Swedish Nuclear Fuel and Waste Management Company, Technical Report TR 82-18.
- Christensen, H., R. Forsyth, L. Lundquist and L.O. Werme. 1990. Radiation induced dissolution of UO_2 , Studsvik Report NS-90185, Studsvik Energiteknik AB, Nykoping, Sweden.
- Clarens, F., J. de Pablo, I. Diaz-Perez, I. Casas, J. Gimenez and M. Rovira. 2004. Formation of studtite during the oxidative dissolution of UO_2 by hydrogen peroxide, *Environ. Sci. Technol.* 38, 6656-6661.
- Cobos, J., D. Papaioannou, J. Spino and M. Coquerelle. 1998. Phase characterization of simulated high burn-up UO_2 fuel, *J. Alloys and Comps.* 271-273, 610-615.
- Cobos, J., T. Wiss, T. Goudes and V.V. Rondinella. 2003. XPS and SEM studies on the corrosion of UO_2 containing plutonium in de-mineralized and carbonated water, *Mat. Res. Soc. Symp. Proc.* 757, 365-375.
- Corbel, C., G. Sattonnay, S. Guilbert, F. Garrido, M-F. Barthe and C. Jegou. 2006. Addition versus radiolytic production effects on aqueous corrosion of UO_2 , *J. Nucl. Mater.* 348, 1-17.
- Cramer, J.J., and J.A.T. Smellie. 1994. Final report of the AECL/SKB Cigar Lake analog study, Atomic Energy of Canada Limited Report, AECL-10851, COG-93-147, SKB TR 94-04.
- Cui, D., J. Low, C.J. Sjostedt, and K. Spahiu. 2004. On Mo-Ru-Tc-Pd-Rh alloy particles extracted from spent fuel and their leaching behavior under repository conditions, *Radiochim. Acta* 92, 551-558.

- Cui, D., K. Spahiu and P. Wersin. 2003. Redox reactions of iron and uranium dioxide in simulated cement pore water under anoxic conditions, *Mat. Res. Soc. Symp. Proc.* 757, 427-432.
- de Pablo, J., I. Casas, F. Clarens, F. El Aamrani and M. Rovira. 2001. The effect of hydrogen peroxide concentration on the oxidative dissolution of unirradiated uranium dioxide, *Mat. Res. Soc. Symp. Proc.* 663, 409-426.
- de Pablo, J., I. Casas, J. Gimenez, F. Clarens, L. Duro and J. Bruno. 2004. The oxidative dissolution mechanism of uranium dioxide. The effect of pH and oxygen partial pressure, *Mat. Res. Soc. Symp. Proc.* 807, 1-6.
- de Pablo, J., I. Casas, J. Gimenez, V. Marti and M.E. Torrero. 1996. Solid surface evolution model to predict uranium release from unirradiated UO_2 and nuclear spent fuel dissolution under oxidizing conditions, *J. Nucl. Mater.* 232, 138-145.
- de Pablo, J., I. Casas, J. Jimenez, M. Molera, M. Rovira, L. Duro and J. Bruno. 1999. The oxidative dissolution mechanism of uranium dioxide. The effect of temperature in hydrogen carbonate medium, *Geochim. et Cosmochim. Acta* 63, 3097-3103.
- de Pablo, J., I. Casas, J. Gimenez, V. Marti and M.E. Torrero. 1996. Solid surface evolution model to predict uranium release from unirradiated UO_2 and nuclear spent fuel dissolution under oxidizing conditions, *J. Nucl. Mater.* 232, 138-145.
- Diaz-Arocas, P., J. Quinones, C. Maffiotte, J. Serrano, J. Garcia, J.R. Almazan and J. Esteban. 1995. Effect of secondary phase formation in the leaching of UO_2 under simulated radiolytic products, *Mat. Res. Soc. Symp. Proc.* 353, 641-646.
- Eary, L.E., and L.M. Cathles. 1983. A kinetic model of UO_2 dissolution in acid, H_2O_2 solutions that includes uranium peroxide hydrate precipitation, *Metal. Trans B.* 14B, 325-334.
- Ekeroth, E., and M. Jonsson. 2003. Oxidation of UO_2 by radiolytic oxidants, *J. Nucl. Mater.* 242-248.
- Ekeroth, E., O. Roth and M. Jonsson. 2006. The relative impact of radiolysis products in radiation induced oxidative dissolution of UO_2 , *J. Nucl. Mater.* 355, 38-46.
- El Aamrani, F., I. Casas, C. Martin, M. Rovira and J. de Pablo. 1998. Effect of iron and canister corrosion products on the dissolution of UO_2 , In *Proceedings Spent Fuel Workshop 1998, Las Vegas, NV.*
- Finch, R.J., and R.C. Ewing. 1991. Alteration of natural uraninite under oxidizing conditions from Shinkolobwe, Katanga, Zaire. A natural analog for the corrosion of spent fuel, *Radiochim. Acta* 52/53, 395-401.
- Finch, R.J., and R.C. Ewing. 1992. The corrosion of uraninite under oxidizing conditions, *J. Nucl. Mater.* 190, 133-156.
- Finch, R.J., E.C. Buck, P.A. Finn and J.K. Bates. 1999. Oxidative corrosion of spent UO_2 fuel in vapour and dripping groundwater at 90°C, *Mat. Res. Soc. Symp. Proc.* 556, 431-438.

- Finch, R.J., J.A. Fortner, E.C. Buck and S.F. Wolf. 2002. Neptunium incorporation into uranium (VI) compounds formed during aqueous corrosion of neptunium-bearing uranium oxide, *Mat. Res. Soc. Symp. Proc.* 713, 647-654.
- Finn, P.A., J.C Hoh, S.F. Wolf, M.T. Surchik, E.C. Buck and J.K Bates. 1997. Spent fuel reaction: The behaviour of the epsilon phase over 3.1 years, *Mat. Res. Soc. Symp. Proc.* 465, 527-534.
- Finn, P.A., J.K. Bates, J.C. Hoh, J.W. Emery, L.D. Hafenrichter, E.C. Buck and M. Gong. 1994. Elements present in leach solutions from unsaturated spent fuel tests, *Mat. Res. Soc. Symp. Proc.* 333, 399-407.
- Forsyth, R. 1997. The SKB spent fuel corrosion programme. An evaluation of results from the experimental programme performed in the Studsvik hot cell laboratory, Swedish Nuclear Fuel and Waste Management Company, Technical Report TR-97-25.
- Fuger, J. 1993. Problems in the thermodynamics of the actinides in relation with the back-end of the nuclear cycle, *J. Nucl. Mater.* 201, 3-14.
- Garisto, F., A. D'Andrea, P. Gierszewski and T. Melnyk. 2004. Third case study- reference data and codes, Ontario Power Generation Report No: 06819-REP-01200-10107-R00.
- Garisto, N.C., and D.M.LeNeveu. 1991. A radionuclide mass-transport model for the performance assessment of engineered barriers in a used nuclear fuel disposal vault, Atomic Energy of Canada Limited Report, AECL-10277.
- Gierszewski, P., J. Avis, N.Calder, A. D'Andrea, F. Garisto, C. Kitson, T.W. Melnyk, K. Wei, and L. Wojcieckowski. 2004. Third case study – Post closure safety assessment, Ontario Power Generation Report No: 06819-REP-01200-10109-R00.
- Gimenez, J., E. Baraj, M. E. Torrero, I. Casas and J. de Pablo. 1996. Effect of H₂O₂, NaClO, and Fe on the dissolution of unirradiated UO₂ in NaCl 5 mol·kg⁻¹. Comparison with spent fuel dissolution experiments, *J. Nucl. Mater.* 238, 64-69.
- Goldik, J.S., H.W. Nesbitt, J.J. Noel and D.W. Shoesmith. 2004. Surface electrochemistry of UO₂ in dilute alkaline hydrogen peroxide solutions, *Electrochim. Acta*, 49, 1699-1709.
- Goldik, J.S., J.J. Noel and D.W. Shoesmith. 2005. The electrochemical reduction of hydrogen peroxide on uranium dioxide electrodes in alkaline solution, *J. Electroanal. Chem.* 582, 241-248.
- Goldik, J.S., J.J. Noel and D.W. Shoesmith. 2006a. Surface electrochemistry of UO₂ in dilute alkaline hydrogen peroxide solutions. Effects of carbonate ions, *Electrochim. Acta*, 51, 3278-3286.
- Goldik, J.S., J.J. Noel and D.W. Shoesmith. 2006b. The effects of simulated fission products in the reduction of hydrogen peroxide on simulated nuclear fuel electrodes, *J. Electrochem. Soc.* 153, E151-E159.

- Goldik, J.S. 2006. The electrochemistry of SIMFUEL in dilute alkaline hydrogen peroxide solutions, PhD Thesis, University of Western Ontario, London, Canada, Chapter 5.
- Grambow, B., A Loida, P. Dressler, H. Geckeis, P. Diaz, J. Gago, I. Casas, J. de Pablo, J. Gimenez and M.E. Torrero. 1994. Reaction of high burnup spent fuel in saline brines at room temperature, Kernforschungszentrum Karlsruhe, Karlsruhe, Germany, KFK-5377.
- Grambow, B., A. Loida, A. Martinez-Esparza, P. Diaz-Arocas, J. de Pablo, G. Marx, J.P. Glatz, K. Lemmens, K. Ollila and H. Christensen. 2000. Source term for performance assessment of spent fuel as a waste form, European Commission, Nuclear Science and Technology Report, EUR 19140 EN.
- Grambow, B., E. Smailos, H. Geckeis, R. Muller and H. Hentschel. 1996. Sorption and reduction of uranium (VI) on iron corrosion products under reducing saline conditions, *Radiochim. Acta* 74, 149-154.
- Grandstaff, D.E. 1976. A kinetic study of the dissolution of uraninite, *Econ. Geol. Bull. Soc. Econ. Geol.* 71, 1493-1506.
- Gray, W.J. 1998. Dissolution rates as a function of burnup and water chemistry, Pacific Northwest National Laboratory, Richland, WA, PNNL-11895.
- Gray, W.J., and C.N. Wilson. 1995. Spent fuel dissolution studies FY 1991-1994, Pacific Northwest National Laboratory, Richland, WA, PNNL-10540.
- Grenthe, I., J. Fuger, R.J. Konings, R.J. Lemire, A.B. Muller, C. Nguyen-Trung and H. Wanner, Chemical thermodynamics of uranium, North Holland, Amsterdam (1992).
- Guillamont, R., T. Fanghanel, I. Grenthe, V. Neck, D. Palmer, and M.H. Rand. 2003. Update on the chemical thermodynamics of uranium, neptunium, plutonium, americium and technetium, OECD-NEA, Chemical Thermodynamics Vol. 5, 182-187, Elsevier, Amsterdam.
- Hastings, I.J. 1982. Structures in irradiated UO₂ fuel from Canadian reactors, Atomic Energy of Canada Limited Report AECL-MISC-249.
- He, H., P.G. Keech, M.E. Broczkowski, J J. Noel and D.W. Shoesmith. 2007. Characterization of the influence of fission product doping on the anodic reactivity of uranium dioxide, accepted for publication in *Can. J. Chem.* May 2007.
- Hiskey, J.B. 1980. Hydrogen peroxide leaching of uranium in carbonate solutions, *Inst. Min. Metall. Tran. Section C89*, C145-C152.
- Hocking, W.H., J.S. Betteridge and D.W. Shoesmith. 1991. The cathodic reduction of dioxygen on uranium oxide in dilute alkaline aqueous solution, Atomic Energy of Canada Limited Report, AECL-10402.
- Hocking, W.H., J.S. Betteridge and D.W. Shoesmith. 1994. The cathodic reduction of oxygen on uranium oxide in dilute alkaline aqueous solution, *J. Electroanal. Chem.* 379, 339-351.

- Hossain, M.M., E. Ekeroth and M. Jonsson. 2006. Effects of HCO_3^- on the kinetics of UO_2 oxidation by H_2O_2 , J. Nucl. Mater. 358, 202-208.
- Hyland, G.J., and J. Ralph. 1983. Electronic contributions to the high temperature thermophysical properties of UO_{2+x} . A critical analysis, High Temp. High Pressure, 15, 179-190.
- Ilin, S.R., K. Spahiu and U-B. Eklund. 2001. Determination of dissolution rates of spent fuel in carbonate solutions under different redox conditions with a flow-through experiment, J. Nucl. Mater. 297, 231-243.
- Jegou, C., V. Broudie, A. Poulesquen and J.M. Bart. 2004. Effects of α and γ - radiolysis of water on alteration of the spent fuel UO_2 nuclear fuel matrix, Mat. Res. Soc. Symp. Proc. 807, 391-396.
- Johnson, L.H., and D.W. Shoesmith. 1988. Spent Fuel. In radioactive waste forms for the future (W.B. Lutze and R.C. Ewing, editors). Elsevier Science Publishers, Amsterdam, Netherlands.
- Johnson, L.H., and P.A. Smith. 2000. The interaction of radiolysis products and canister corrosion products and the implications for spent fuel dissolution and radionuclide transport in a repository for spent fuel, Nagra, Wettingen, Switzerland, Technical Report 00-04.
- Johnson, L.H., D.M. Leneveu, D.W. Shoesmith, D.W. Oscarson, M.N. Gray, R.J. Lemire, and N.C. Garisto. 1994. The disposal of Canada's nuclear fuel waste: the vault model for post closure assessment, Atomic Energy of Canada Limited Report AECL-10714, COG-94-4.
- Johnson, L.H., D.M. Leneveu, F. King, D.W. Shoesmith, M. Kolar, D.W. Oscarson, S. Sunder, C. Onofrei, and J.L. Crosthwaite. 1996. The disposal of Canada's nuclear fuel waste: A study of post closure safety of in-room emplacement of used CANDU fuel in copper containers in permeable plutonic rock volume 2: Vault model. Atomic Energy of Canada Limited Report, AECL-11494-2, COG-95-552-2.
- Jonsson, M., E. Ekeroth and O. Roth. 2004. Dissolution of UO_2 by one-and two- electron oxidants, Mat. Res. Soc. Symp. Proc. 807, 77-82.
- Jonsson, M., F. Nielsen, O. Roth, E. Ekeroth, S. Nilsson and M.M Hossain. 2006. Radiation induced spent nuclear fuel dissolution under deep repository conditions, submitted to Environ. Sci. Technol.
- Kim, J.D., S.I. Pyun, T.H. Yang and J.B. Ju. 1995. A study of the mechanism of oxygen reduction on bare palladium in 0.1M LiOD solution using Pt-Ring-Pd disc electrode, J. Electroanal. Chem. 383,161-166.
- King, F., and S. Stroes-Gascoyne. 2000. An assessment of the long-term corrosion behavior of C-steel and the impact of redox conditions inside a nuclear fuel waste disposal container, Ontario Power Generation Report No: 06819-REP-01200-10028-R00.

- King, F., and D.W. Shoesmith. 2004. Electrochemical studies of the effect of H₂ on UO₂ dissolution, Swedish Nuclear Fuel and Waste Management Company, Technical Report TR-04-20.
- King, F., and M. Kolar. 1996. Modeling the consumption of oxygen by container corrosion and reaction with Fe (II), Mat. Res. Soc. Symp. Proc. 412, 547-554.
- King, F., and M. Kolar. 1999. Prediction of the effects of α -radiolysis, precipitation and Redox Reactions with Fe and Fe (II) on the Dissolution of UO₂ using the mixed potential model of Fuel Dissolution (MPM Version 1.1), Ontario Power Generation Report No: 06819-REP-01200-10014-R00.
- King, F., and M. Kolar. 2000. Analysis of the effect of cladding on the oxidative dissolution of used nuclear fuel using the mixed-potential model of fuel dissolution (MPM Version 1.2), Ontario Power Generation Report No: 06819-REP-01200-10022-R00.
- King, F., and M. Kolar. 2000. The copper container corrosion model used in AECL'S second case study. Ontario Power Generation No: 06819-REP-01200-10041-R00.
- King, F., and M. Kolar. 2001a. Mixed potential model simulations of the effects of porous film formation on the dissolution of used fuel (MPM Version 1.3), Ontario Power Generation Report No: 06819-REP-01300-10019-R00.
- King, F., and M. Kolar. 2001b. An improved C-steel corrosion model for the mixed-potential model for used fuel dissolution (MPM Version 1.4), Ontario Power Generation Report No: 06819-REP-01300-10027-R00.
- King, F., and M. Kolar. 2002b. Sensitivity analysis of the factors affecting the effective G-value, G_{EFF}, in the mixed potential model for used fuel dissolution, Ontario Power Generation Report No: 06819-REP-01300-10044-R00.
- King, F., and M. Kolar. 2002a. Validation of the mixed-potential model for used fuel dissolution against experimental data, Ontario Power Generation Report No: 06819-REP-01200-10077-R00.
- King, F., M.J. Quinn and N.H. Miller. 1999. The effect of hydrogen and gamma radiation on the oxidation of UO₂ in 0.1 mol·dm⁻³ NaCl solution, Swedish Nuclear Fuel and Waste Management Company, Technical Report TR-99-27.
- Kolar, M., and F. King. 2003. The mixed-potential model for UO₂ dissolution, MPM Version V1.3 and V1.4, Ontario Power Generation Report No: 06819-REP-01200-10104-R00.
- Kubatko, K-A., K.B. Hilean, A. Navrotsky and P.C. Burns. 2003. Stability of peroxide-containing uranyl minerals, Science 302, 1191-1193.
- Laverne, J.A., and L. Tandon. 2003. H₂ production in the radiolysis of water on UO₂ and other oxides, J. Phys, Chem. B. 107, 13623-13628.

- Lee, C.T., Z. Qin, M. Odziemkowski and D.W. Shoesmith. 2005. The influence of groundwater anions on the impedance behavior of carbon steel corroding under anoxic conditions, *Electrochim. Acta* 51, 1558-1568
- Lemire, R.J., and P.R. Tremaine. 1980. Uranium and plutonium equilibria in aqueous solutions to 200°C, *J. Chem. Eng. Data*, 25, 361-370.
- Lemire, R.J., and F.Garisto. 1989. The Solubility of U, Np, Pu, Th, and Tc in a geological disposal vault for used fuel, *Atomic Energy of Canada Report*, AECL-10009.
- Loida, A., B. Grambow and H. Geckeis. 1996. Anoxic corrosion of various high burn-up spent fuel samples, *J. Nucl. Mater.* 238, 11-22.
- Loida, A., B. Grambow and H. Geckeis. 2001. Congruent and incongruent radionuclide release during matrix dissolution of partly oxidized high burn-up spent fuel, *Mat. Res. Soc. Symp. Proc.* 663, 417-426.
- Loida, A., M. Kelm, B. Kienzer, H. Geckeis and A. Bauer. 2006. The effect of near field constraints on the corrosion behavior of high burn-up spent fuel, *Mat. Res. Soc. Symp. Proc.* 932, 473-480.
- Lucuta, P.G., R.A. Verrall, H.J. Matzke and B.J.F. Palmer. 1991. Microstructural features of SIMFUEL-simulated high burn-up UO₂-based nuclear fuel, *J. Nucl. Mater* 178, 48-60.
- Luht, J.L.M. 1998. Anodic dissolution of uranium dioxide in simple electrolyte solutions and simulated ground waters, M. Sc. Thesis, University of Manitoba, Winnipeg, MB.
- Maak, P. 2003. Development of a used fuel container for nuclear fuel waste. *Mat. Res. Soc. Symp. Proc.* 807, 447.
- Martinovic, J.M., D.B. Sepa, M.V. Vojnovic and A. Damjanovic. 1988. Kinetics of electrochemical reduction of oxygen at rhodium, *Electrochim. Acta* 33, 1267-1272.
- Matzke, H., P.G. Lucuta and R.A. Verrall. 1991. Formation and behaviour of barium silicates in UO₂-based SIMFUEL, *J. Nucl. Mater.* 185, 292-296.
- McEachern, R.J., and P. Taylor. 1998. A review of the oxidation of uranium dioxide at temperatures below 400°C, *J. Nucl. Mater.* 254, 87-121.
- McMurry, J., D.A. Dixon, J.D Garroni, B.M. Ikeda, S. Stroes-Gascoyne, P. Baumgartner and T.W. Melnyk. 2003. Evolution of a Canadian deep geologic repository: base scenario. *Ontario Power Generation Report No: 06819-REP-01200-10092-R00.*
- Mennecart, T., B. Grambow, M. Fattahi, G. Blondiaux, Z. Andriambololona. 2004. Effect of alpha radiolysis on UO₂ dissolution under reducing conditions, *Mat. Res. Soc. Symp. Proc.* 807, 403-408.
- Neck, V., and J.I. Kim. 2001. Solubility and hydrolysis of tetravalent actinides, *Radiochim. Acta* 89, 1-16.

- Nicol, M.J., and C.R.S. Needes. 1973. The mechanism of the anodic dissolution of uranium dioxide, Nat. Inst. Met. Repub. S. Africa, Report No: 7079.
- Nielsen, F., and M. Jonsson. 2006. Geometric α - and β - dose rate distributions and production rates of radiolysis products in water in contact with spent nuclear fuel, J. Nucl. Mater. 359, 1-7.
- Nilsson, S., and M. Jonsson. 2007. On the catalytic effects of $\text{UO}_2(\text{s})$ and $\text{Pd}(\text{s})$ on the reaction between H_2O_2 and H_2 in aqueous solution, J. Nucl. Mater, in press.
- Novak, J., and I.J. Hastings. 1991. Ontario Hydro experience with extended burnup power reactor fuel. Atomic Energy of Canada Limited Report, AECL-10388.
- Nuclear Waste Management Organization (NWMO). 2005. Choosing a way forward: The future management of Canada's used nuclear fuel, www.nwmo.ca.
- Office of Civilian Radioactive Waste Management. 2004. CSNF Waste Form Degradation: Summary Abstraction ANL-EBS-MD-000015 REV.02
- Ollila, K., Y. Albinsson, V. Oversby and M. Cowper. 2003. Dissolution rates of unirradiated UO_2 , UO_2 doped with ^{233}U and spent fuel under normal atmospheric conditions and under reducing conditions using an isotope dilution method, Swedish Nuclear Fuel and Waste Management Company, Technical Report TR-03-13.
- Oversby, V.M. 1999. Uranium dioxide, SIMFUEL, and spent fuel dissolution rates- A review of published data, Swedish Nuclear Fuel and Waste Management Company, Technical Report TR-99-22.
- Paquette, J. and R.J. Lemire. 1981. A description of the chemistry of aqueous solutions of uranium and plutonium to 200°C using potential pH diagrams, Nucl. Sci. Eng. 79, 26-48.
- Parks, G.A., and D.C. Pohl. 1988. Hydrothermal solubility of uraninite, Geochim. Cosmochim. Acta 52, 863-875.
- Pastina, B., and J.A. Laverne. 2001. Effect of molecular hydrogen on hydrogen peroxide in water radiolysis, J. Phys. Chem. A 105, 9316-9322.
- Petrik, N.G., A.B. Alexandrov and A.I. Vall. 2001. Interfacial energy transfer during gamma radiolysis of water on the surface of ZrO_2 and some other oxides, J. Phys. Chem. B. 105, 5935-5944.
- Poinssot, C., C. Ferry, M. Kelm, B. Grambow, A. Martinez-Esparza, L. Johnson, Z. Andriambololona, J. Bruno, C. Cachoir, J-M. Cavendon, H. Christensen, C. Corbel, C. Jegou, K. Lemmens, A. Loida, P. Lovera, F. Miserque, J. de Pablo, A. Poulesquen, J. Quinones, V. Rondinella, K. Spahiu and D. Wegen. 2005. Final report of the European project spent fuel stability under repository conditions. European Commission Report CEA-R-6093.

- Quinones, J., J.A. Serrano, P. Diaz-Arocas, J.L. Rodriguez-Almazan, J. Cobos, J.A. Esteban and A. Martinez-Esparza. 2001. Influence of container base material (Fe) on SIMFUEL leaching behaviour, *Mat. Res. Soc. Symp. Proc.* 663, 435-439.
- Rai, D., A.R. Felmy and J.L. Ryan. 1990. Uranium (IV) hydrolysis constants and solubility product of $\text{UO}_2 \cdot x\text{H}_2\text{O}$ (am), *Inorg. Chem.* 29, 260-264.
- Rai, D., M. Yui and D.A. Moore. 2003. Solubility and solubility product at 22°C of UO_2 (c) precipitated from aqueous U (IV) solutions, *J. Solution Chem.* 32, 1-17.
- Rollin, S., K. Spahiu and U.B. Eklund. 2001. Determination of dissolution rates of spent fuel in carbonate solutions under different redox conditions with a flow-through experiment, *J. Nucl. Mater.* 297, 231-243.
- Rudnicki, J.D., R. Russo and D.W. Shoesmith. 1994. Photothermal deflection spectroscopy investigation of uranium dioxide oxidation, *J. Electroanal. Chem.* 372, 63-74.
- Santos, B.G., H.W. Nesbitt, J.J. Noel and D.W. Shoesmith. 2004. X-ray photoelectron spectroscopy study of anodically oxidized SIMFUEL surfaces, *Electrochim. Acta*, 49, 1863-1873.
- Santos, B.G., J.J. Noel and D.W. Shoesmith. 2006. The effect of pH on the anodic dissolution of SIMFUEL (UO_2), *J. Electroanal. Chem.* 586, 1-11.
- Santos, B.G., J.J. Noel and D.W. Shoesmith. 2006a. The influence of calcium ions on the development of acidity in corrosion product deposits on SIMFUEL (UO_2), *J. Nucl. Mater.* 350, 320-331.
- Santos, B.G., J.J. Noel and D.W. Shoesmith. 2006b. The influence of silicate on the development of acidity in corrosion product deposits on SIMFUEL (UO_2), *Corros. Sci.* 48, 3852-3868.
- Santos, B.G., J.J. Noel and D.W. Shoesmith. 2006c. The influence of potential on the anodic dissolution of SIMFUEL (UO_2), *Electrochim. Acta* 51, 4157-4166.
- Shoesmith, D.W. 2000. Fuel corrosion processes under waste disposal conditions, *J. Nucl. Mater.* 282, 1-31.
- Shoesmith, D.W., and F. King. 1998. A mixed potential model for the prediction of the effects of alpha radiolysis, precipitation and redox processes on the dissolution of used nuclear fuel, Ontario Power Generation Report No: 06819-REP-01200-0038-R00.
- Shoesmith, D.W., and S. Sunder. 1991. An electrochemistry-based model for the dissolution of UO_2 , Atomic Energy of Canada Report, AECL-10488.
- Shoesmith, D.W., and S. Sunder. 1992. The prediction of nuclear fuel (UO_2) dissolution rates under waste disposal conditions, *J. Nucl. Mater.* 190, 20-35.

- Shoesmith, D.W., J.J. Noel, and F. Garisto. 2004. An experimental basis for a mixed potential model for nuclear fuel corrosion within a failed nuclear waste container, *Mat. Res. Soc. Symp. Proc.* 824, 81-88.
- Shoesmith, D.W., J.C. Tait, S. Sunder, R.E. Russo and J.D. Rudnicki. 1996. Factors affecting the differences in reactivity and dissolution rate between UO_2 and spent nuclear fuel. Atomic Energy of Canada Limited Report, AECL-11515, COG-95-581.
- Shoesmith, D.W., J.J. Noel and F. Garisto. 2004. An experimental basis for a mixed potential model for nuclear fuel corrosion within a failed nuclear waste container, *Mat. Res. Soc. Symp. Proc.* 824, 81-88.
- Shoesmith, D.W., J.J. Noel, Z. Qin, C.T. Lee, J.S. Goldik, B.G. Santos and M.E. Broczkowski. 2005. Corrosion of nuclear fuel (UO_2) inside a failed nuclear waste container, Ontario Power Generation Report No: 06819-REP-01200-10145-R00.
- Shoesmith, D.W., M. Kolar and F. King. 2003. A mixed potential model to predict fuel (uranium dioxide) corrosion within a failed nuclear waste container, *Corrosion* 59, 802-816.
- Shoesmith, D.W., S. Sunder and J.C. Tait. 1998. Validation of an electrochemical model for the oxidative dissolution of used CANDU fuel, *J. Nucl. Mater.* 257, 89-98.
- Shoesmith, D.W., S. Sunder and W.H. Hocking. 1994. Electrochemistry of UO_2 nuclear fuel, in *Electrochemistry of Novel Materials* (edited by J. Lipkowski and P.N. Ross), VCH Publishers, New York, Chapter 6, 297-337.
- Shoesmith, D.W., S. Sunder, M.G. Bailey and D.G. Owen. 1983. Anodic oxidation of UO_2 , III. Electrochemical studies in carbonate solutions, In *Passivity of Metals and Semiconductors, Proceedings of the Fifth International Symposium on Passivity, Bombannes, France* (edited by M. Froment) May 1983, Elsevier, Amsterdam, 125-130.
- Shoesmith, D.W., S. Sunder, M.G. Bailey and G.J. Wallace. 1984. Anodic oxidation of UO_2 . IV. Electrochemical and X-ray photoelectron spectroscopic studies in carbonate solutions, *Appl. Surf. Sci.* 20, 39-57.
- Shoesmith, D.W., S. Sunder, M.G. Bailey and G.J. Wallace. 1989. Corrosion of nuclear fuel in oxygenated solutions, *Corros. Sci.* 29, 1115-1128.
- Shoesmith, D.W., S. Sunder, M.G. Bailey and N.H. Miller. 1996. Oxidation and dissolution (corrosion) of used fuel electrodes in aqueous perchlorate and carbonate solutions, *J. Nucl. Mater.* 227, 287-299.
- Shoesmith, D.W., W.H. Hocking and J.S. Betteridge. 2001. The influence of UO_2 fuel composition on its corrosion behavior under waste disposal conditions, Ontario Power Generation Report No: 06819-REP-01200-10052-R00.
- Smart, N.R., D.J. Blackwood, and L. Werme. 2002a. Anaerobic corrosion of carbon steel and cast Iron in artificial groundwater. Part I- Electrochemical aspects, *Corrosion* 58, 547-559.

- Smart, N.R., D.J. Blackwood and L. Werme. 2002b. Anaerobic corrosion of carbon steel and cast iron in artificial groundwater. Part II – Gas generation, *Corrosion*, 58, 627-637.
- Spahiu, K., J. Devoy, D. Cui and D. Lundstrom. 2004. The reduction of U(VI) by near field hydrogen in the presence of $\text{UO}_2(\text{s})$. *Radiochim. Acta* 92, 597-603.
- Spahiu, K., L. Werme and U.B. Eklund. 2000. The influence of near field hydrogen on actinide solubilities and spent fuel leaching, *Radiochim. Acta* 88, 507-511.
- Stroes-Gascoyne, S., F. King and J.S. Betteridge. 2002a. The effects of alpha-radiolysis on UO_2 dissolution determined from electrochemical experiments with ^{238}Pu -doped UO_2 , Ontario Power Generation Report 06819-REP-01300-10030-R00.
- Stroes-Gascoyne, S., F. King, J.S. Betteridge and F. Garisto. 2002b. The effects of alpha-radiolysis on UO_2 dissolution determined from electrochemical experiments with ^{238}Pu -doped UO_2 , *Radiochim. Acta* 90, 603-609.
- Stroes-Gascoyne, S., F. Garisto and J.S. Betteridge. 2005. The effects of alpha-radiolysis on UO_2 dissolution determined from batch experiments with ^{238}Pu -doped UO_2 , *J. Nucl. Mater.* 346, 5-15.
- Stultz, J., M.T. Paffet and S.A. Joyce. 2004. Thermal evolution of hydrogen following water adsorption on UO_2 (100), *J. Phys. Chem. B.*, 108, 2362-2364.
- Stumm, W. (editor). 1990. Aquatic chemical kinetics. Reaction rates of processes in natural waters, John Wiley, New York, NY.
- Sunder, S. 1995. Alpha, beta and gamma dose rates in water in contact with used CANDU UO_2 fuel, Atomic Energy of Canada Limited Report, AECL-11380, C06- 95-340.
- Sunder, S., D.W. Shoesmith, and N.H. Miller. 1997. Oxidation and dissolution of nuclear fuel (UO_2) by the products of the alpha radiolysis of water, *J. Nucl. Mater.* 244, 66-74.
- Sunder, S., D.W. Shoesmith, H. Christensen and N.H. Miller. 1992. Oxidation of UO_2 fuel by the products of gamma radiolysis of water, *J. Nucl. Mater* 190, 78-86.
- Sunder, S., D.W. Shoesmith, M. Kolar and D.M. Leneveu. 1997. Calculation of used nuclear fuel dissolution rates under anticipated Canadian waste vault conditions, *J. Nucl. Mater.* 250, 118-130.
- Sunder, S., G.D. Boyer and N.H. Miller. 1990. XPS studies of UO_2 oxidation by alpha radiolysis of water at 100°C , *J. Nucl. Mater.* 175, 163-169.
- Sunder, S., N.H. Miller and D.W. Shoesmith. 2004. Corrosion of uranium dioxide in hydrogen peroxide solutions, *Corros. Sci.* 46, 1095-1111.
- Sutton, H.C., and C.C. Winterbourn. 1989. On the participation of higher oxidation states of iron and copper in Fenton reactions, *Free Rad. Biol. Med.* 6, 53-60

- Tait, J.C., and J.M Luht. 1997. Dissolution rates of uranium from unirradiated UO_2 and uranium and radionuclides from used CANDU fuel using the single-pass flow-through apparatus. Ontario Hydro Report No: 06819-REP-01200-0006-R00.
- Tait, J.C., and L.H. Johnson. 1986. Computer modeling of alpha radiolysis of aqueous solutions in contact with used UO_2 fuel. Proceedings 2nd International Conference on Radioactive Waste Management, Winnipeg, MB, September 7-11, 1986, Canadian Nuclear Society, Toronto, 611-615.
- Tait, J.C., H. Roman and C.A. Morrison. 2000. Characteristics and radionuclide inventories of used fuel from OPG nuclear generating stations, Volumes 1 and 2, Ontario Power Generation Report No: 06819-REP-01200-10029-R00.
- Tamura, H., K. Goto and M. Nagayama. 1976. The effect of ferric hydroxide on the oxygenation of ferrous ions in neutral solutions, *Corros. Sci.* 16, 197-207.
- Thomas, L.E., R.E. Einziger and H.C. Buchanan. 1993. Effect of fission products on air-oxidation of LWR spent fuel, *J. Nucl. Mater.* 201, 310-319.
- Torrero, M.E., E. Baraj, J. de Pablo, J. Gimenez and I. Casas. 1997. Kinetics of corrosion and dissolution of uranium dioxide as a function of pH, *Int. J. Chem. Kinet.* 29, 261-267.
- Vracar, Lj.M., D.B. Sepa and A. Damjanovic. 1987. Palladium electrode in oxygen-saturated solutions, *J. Electrochem. Soc.* 134, 1695-1697.
- Vracar, Lj.M., D.B. Sepa and A. Damjanovic. 1986. Palladium electrode in oxygen-saturated aqueous solutions, *J. Electrochem. Soc.* 133, 1835-1839.
- Werme, L., and R. Forsyth. 1989. The SKB spent fuel corrosion program. Status reports 1988. Swedish Nuclear Fuel and Waste Management Company, Technical Report TR-89-14.
- Werme, L., L.H. Johnson, V.M. Oversby, F. King, K. Spahiu, B. Grambow and D.W. Shoesmith. 2004. Spent fuel performance under repository conditions: A model for use in SR-Can, Swedish Nuclear Fuel and Waste Management Company, Technical Report TR-04-19.
- Wilson, C.N., and W.J. Gray. 1990. *Mat. Res. Soc. Symp. Proc.* 176, 489.
- Winter, P.W. 1989. The electronic transport properties of UO_2 , *J. Nucl. Mater.* 161, 38-43.
- Wren, J.C., D.W. Shoesmith and S. Sunder. 2005. Corrosion behavior of uranium dioxide in alpha radiolytically decomposed water, *J. Electrochem. Soc.* 152, B470-B481.
- Wronkiewicz, D.J. 1999. Uranium: Mineralogy, Geochemistry and the Environment, *Reviews in Mineralogy and Geochemistry*, Mineralogical Society of America, Washington, D.C. 38, 475.
- Wronkiewicz, D.J., J.K. Bates, S.F. Wolf and E.E. Buck. 1996. Ten-year results from unsaturated drip tests with UO_2 at 90°C: Implications for the corrosion of spent nuclear fuel, *J. Nucl. Mater.* 238, 78-95.

Wronkiewicz, D.J., J.K. Bates, T.J. Gerding, E. Veleckis and B.S. Tani. 1992. Uranium release and secondary phase formation during unsaturated testing of UO_2 at 90°C , J. Nucl. Mater. 190, 107-127.

Yajima, T., Y. Kawamura and S. Ueta. 1995. Uranium (IV) solubility and hydrolysis constants under reducing conditions, Mat. Res. Soc. Symp. Proc. 353, 1137-1142.